Glycosphingolipids of the model fungus *Aspergillus nidulans*: characterization of GIPCs with oligo-α-mannose-type glycans

Beau Bennion,* Chaeho Park,† Matthew Fuller,[1,†] Rebecca Lindsey,§ Michelle Momany,§ Richard Jennemann, and Steven B. Levery[2,*]**

Department of Chemistry,* University of New Hampshire, Durham, NH 03824-3598; The Complex Carbohydrate Research Center and Department of Biochemistry and Molecular Biology,† and Department of Plant Biology,§ University of Georgia, Athens, GA 30602-7229; and Abteilung für Zelluläre und Molekuläre Pathologie,** Deutsches Krebsforschungszentrum-Heidelberg, Im Neuenheimer Feld 280, D69120, Heidelberg, Germany

Abstract ***Aspergillus nidulans* is a well-established nonpathogenic laboratory model for the opportunistic mycopathogen, *A. fumigatus*. Some recent studies have focused on possible functional roles of glycosphingolipids (GSLs) in these fungi. It has been demonstrated that biosynthesis of glycosylinositol phosphorylceramides (GIPCs) is required for normal cell cycle progression and polarized growth in *A. nidulans* (Cheng, J., T.-S. Park, A. S. Fischl, and X. S. Ye. 2001. *Mol. Cell Biol.* 21: 6198–6209); however, the structures of *A. nidulans* GIPCs were not addressed in that study, nor were the functional significance of individual structural variants and the downstream steps in their biosynthesis. To initiate such studies, acidic GSL components (designated An-2, -3, and -5) were isolated from *A. nidulans* and subjected to structural characterization by a combination of one-dimensional (1-D) and 2-D NMR spectroscopy, electrospray ionization-mass spectrometry (ESI-MS), ESI-MS/collision-induced decomposition-MS (MS/CID-MS), ESI-pseudo-[CID-MS]^2, and gas chromatography-MS methods. All three were determined to be GIPCs, with mannose as the only monosaccharide present in the headgroup glycans; An-2 and An-3 were identified as di- and trimannosyl inositol phosphorylceramides (IPCs) with the structures Manα1→3Manα1→2Ins1-P-1Cer and Manα1→3(Manα1→6)Manα1→2Ins1-P-1Cer, respectively (where Ins = *myo*-inositol, P = phosphodiester, and Cer = ceramide). An-5 was partially characterized, and is proposed to be a pentamannosyl IPC, based on the trimannosyl core structure of An-3.**—Bennion, B., C. Park, M. Fuller, R. Lindsey, M. Momany, R. Jennemann, and S. B. Levery. **Glycosphingolipids of the model fungus *Aspergillus nidulans*: characterization of GIPCs with oligo-α-mannose-type glycans. *J. Lipid Res.* 2003.** 44: **2073–2088.**

Supplementary key words glycolipid • mass spectrometry • tandem mass spectrometry • collision-induced dissociation • electrospray ionization • NMR spectroscopy • *Aspergillus fumigatus*

Manuscript received 5 May 2003 and in revised form 29 July 2003.

Published, JLR Papers in Press, August 16, 2003.
DOI 10.1194/jlr.M300184-JLR200

A dramatic increase in the frequency of severe mycotic infections during the past two decades has accompanied the growth in populations of immunosuppressed or immunocompromised individuals, including those with acquired immune deficiency due to human immunodeficiency virus infection, recipients of organ and tissue transplants, and patients with leukemias or other cancers (1–5). As with a variety of other microbial infections, reports of resistance to available therapeutic agents have become a major concern for public health clinicians (6–9). The most commonly occurring mycotic infections are those with *Aspergillus* (usually *A. fumigatus* and *A. flavus*), *Candida* (chiefly *C. albicans*), and *Cryptococcus* (chiefly *C. neoformans*); a wide variety of other species, including some that until recently were not thought of as pathogenic, have also been detected with increasing frequency in disseminated mycoses (10–12).

These circumstances have created an urgent need for new antifungal therapeutic and diagnostic agents, and, by extension, an imperative to identify components that are not only critical to the fungal life cycle and infectivity but that also contain structural elements distinct from those of the host. Investigations of glycosphingolipid (GSL) biosynthesis and function in *Saccharomyces cerevisiae* and other fungi have established that GSLs are essential components of the fungal cell membrane (13–15). These studies have

Abbreviations: Cat, cation; CID, collision-induced dissociation; COSY, correlation spectroscopy; ESI, electrospray ionization; GC, gas chromatography; GIPC, glycosylinositol phosphorylceramide; GSL, glycosphingolipid; HPTLC, high-performance thin-layer chromatography; MS, mass spectrometry; TOCSY, total correlation spectroscopy; TOF, time-of-flight.

[1] Present address of M. Fuller: School of Biology, Georgia Institute of Technology, Atlanta, GA 30332.

[2] To whom correspondence should be addressed.
e-mail: slevery@cisunix.unh.edu

focused on glycosylinositol phosphorylceramides (GIPCs), a family of compounds widely distributed among fungi but not found in mammalian cells or tissues (15) (see **Scheme 1**). Fungal components or metabolites that interact strongly with the host immune system are of particular interest, and there is ample evidence that GIPCs can interact with the mammalian immune system, in particular where they present oligosaccharide epitopes not shared with mammalian glycoconjugates (16–21).

Information about GIPC biosynthesis and function has been emerging at an increasing rate, due to generation of a variety of *Saccharomyces* strains mutated with respect to sphingolipid synthesis, the completion of the yeast genome sequence, and the availability of inhibitors of various steps in the GIPC biosynthetic pathway (13–15, 22). Synthesis of inositol phosphorylceramide (IPC), an obligate intermediate in GIPC catabolism, appears to be required for normal growth of *S. cerevisiae* (23). The IPC synthases are believed to be coded by orthologous *AUR1/IPC1* genes discovered in *S. cerevisiae*, *Schizosaccharomyces pombe*, *Candida* spp., *Aspergillus* spp., and *C. neoformans* (24–29), and a number of inhibitors of this reaction have been discovered (30–32). These appear to be very useful tools for studying GIPC biosynthesis and function, as well as offering promise as antifungal agents, insofar as they are highly toxic to many fungi but exhibit low toxicity in mammals (33). Disruption of the *AUR1* gene in *S. cerevisiae* and *S. pombe* results in morphological changes, disappearance of microtubules, abnormal deposition of chitin, and cessation of growth (25, 29). More recently, Luberto et al. (34) observed that downregulation of the *IPC1*-encoded IPC synthase in *C. neoformans* significantly lowered the expression of certain virulence traits, as well as impairing intracellular growth in an in vitro murine macrophage model and pathogenicity in an established rabbit in vivo model. Using both *AUR1* gene disruption and IPC synthase inhibition, Cheng et al. (35) demonstrated convincingly that GIPC biosynthesis is required for normal cell cycle progression and polarized growth in *Aspergillus nidulans* (*Emericella nidulans*). We have also investigated GSL biosynthesis and function in *A. nidulans* (36), because it is an established nonpathogenic model for the opportunistic mycopathogen, *A. fumigatus* (37–41). However, the structures of the GIPCs in *A. nidulans* have not been determined, nor have the possible functional significance of individual GIPC variants and the downstream steps in their biosynthesis been addressed. In this work, we characterized the major GIPC components of *A. nidulans* using one-dimensional (1-D) and 2-D NMR spectroscopy, electrospray ionization-mass spectrometry (ESI-MS); ESI-MS/collision-induced dissociation (CID)-MS; and ESI-pseudo-$[CID\text{-}MS]^2$ in a hybrid ESI-quadrupole/time-of-flight-MS (ESI-Qq/oa-TOF-MS) instrument; and gas chromatography-mass spectrometry (GC-MS). The proposed GIPC structures are all oligo-α-mannose ("high-mannose") GIPCs based on the core Manα3Manα2Ins1P1Cer (Ins = *myo*-inositol; *P* = phosphodiester; Cer = ceramide).

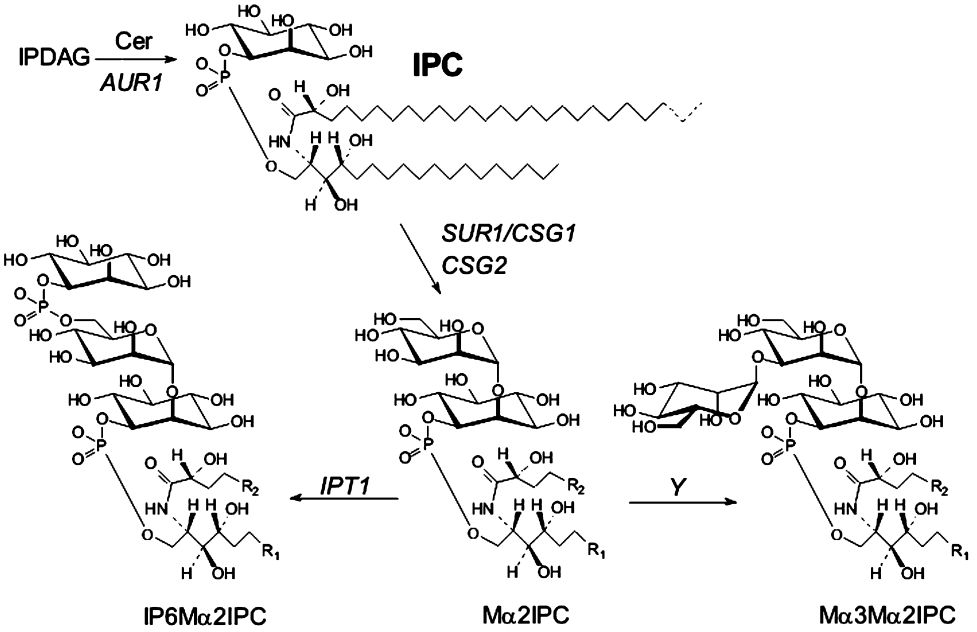

Scheme 1. Biosynthesis of fungal glycosylinositol phosphorylceramides (GIPCs) starting with the transfer of *myo*-inositol-1-O-phosphate (IP) from the diacylglycerol (DAG) moiety of phosphatidylinositol to ceramide, catalyzed by *AUR1* gene-encoded inositol phosphorylceramide (IPC) synthase. Common intermediate Manα1→2InsPCer (Mα2IPC) is next synthesized by the action of Manα2-T (encoded by either *SUR1/CSG1* or *CSG2*, or both). In *S. cerevisae*, *IPT1*-encoded protein transfers a second mole of *myo*-inositol-1-O-phosphate from phosphatidylinositol to Mα2IPC (left arrow). In many other fungi, an as yet unknown Manα3-T (*Y*) transfers a second α-Man residue to Mα2IPC to make a common intermediate Mα3Mα2IPC (right arrow).

EXPERIMENTAL PROCEDURES

Fungal isolate and growth conditions

A. nidulans FGSC strain A28 was used for all preparations. Approximately 5×10^9 spores were inoculated to 200 ml or 1 l complete medium (1% glucose, 0.2% peptone, 0.1% yeast extract, 0.1% casamino acids, nitrate salts, trace elements, and 0.01% vitamins, pH 6.5; trace elements, vitamins, nitrate salts, and amino acid supplements are described in the appendix to Kafer (42), incubated at 30 or 37°C with shaking (200 rpm) for 24 h, filtered, and processed as described. Yields were 6–8 g wet weight per 200 ml medium, or 25–35 g wet weight per 1 l medium.

Solvents for extraction and anion exchange chromatography

Solvent A, isopropanol-hexane-water (55:25:20; v/v/v, upper phase discarded); solvent B, chloroform-methanol (1:1; v/v); solvent C, chloroform-methanol-water (30:60:8; v/v/v).

High-performance thin-layer chromatography

Analytical high-performance thin-layer chromatography (HPTLC) was performed on silica gel 60 plates (E. Merck, Darmstadt, Germany) using chloroform-methanol-water (50:47:14; v/v/v, containing 0.038% w/v $CaCl_2$; solvent D) as mobile phase. Lipid samples were dissolved in solvent A and applied by streaking from 5 μl Micro-caps (Drummond, Broomall, PA). Detection was made by Bial's orcinol reagent [orcinol 0.55% (w/v) and H_2SO_4 5.5% (v/v) in ethanol-water (9:1; v/v)]. The plate was sprayed and heated briefly to ~200–250°C.

Extraction and purification of GSLs

Extraction and purification of GSLs were carried out as described previously (19, 36, 43), but with some modifications and additional steps introduced for the purpose of reducing earlier in the protocol the amounts of irrelevant substances to be dealt with. Briefly, GSLs were extracted by homogenizing mycelia (25–35 g wet weight) in an Omni-mixer (Sorvall Inc., Wilmington, DE) three times with 200 ml of solvent A and three times with 200 ml of solvent B. The six extracts were pooled, dried on a rotary evaporator, dialysed against water, and lyophilized. The dried residue was partitioned between water and 1-butanol presaturated with water (200 ml each) with vigorous shaking in a separatory funnel. The lower (water) layer was removed and similarly extracted three more times with equal volumes of water-saturated 1-butanol. The four 1-butanol extracts were combined in a round-bottom flask, evaporated to dryness, resuspended in a minimal volume of solvent C, and applied to a column of DEAE-Sephadex A-25 (Ac^- form). Neutral GSLs were eluted with 5 vol of solvent C. Acidic GSLs were eluted with 5 vol of 0.5 M sodium acetate in MeOH. The acidic fraction was dried, dialyzed exhaustively against deionized water, redried, and treated with 20 ml methanol-water-1-butanol (4:3:1; v/v/v) containing 25–30% methylamine at 55°C for 4 h (flask tightly stoppered), with occasional agitation. After removal of the reagent solution by rotary evaporation, the acidic lipids were further fractionated by repetitive preparative-scale HPLC, employing columns of either 60 cm × 4.6 mm Iatrobeads (6RS-8010; Iatron Chemical Co., Tokyo, Japan) or 50 cm × 4.6 mm Sphereclone (Phenomenex, Torrance, CA) 10 μm porous spherical silica. The mobile phase was a 2-propanol-hexane-water gradient programmed from 55:40:5 to 55:25:20 (v/v/v) over 120 min, followed by isocratic elution for 40 min; flow rate 0.5 ml/min. Generally, 40 × 2 ml fractions were collected for first-stage purifications, and 80 × 1 ml fractions were collected for second-stage purifications, where required. The identity and purity of each fraction were assessed by analytical HPTLC using solvent D, as above, and by 1-D ^{1}H-NMR spectroscopy before further characterization by the full range of NMR and MS techniques described below.

1-D ^{1}H and 2-D ^{1}H-^{1}H and ^{1}H-^{13}C nuclear magnetic resonance spectroscopy

Samples of underivatized GIPC (~0.5−1.0 mg) were deuterium exchanged by repeated lyophilization from D_2O, and then dissolved in 0.5 ml DMSO-d_6/2% D_2O (44, 45) for NMR analysis. 1-D ^{1}H-NMR, 2-D ^{1}H-^{1}H-gradient-enhanced correlation spectroscopy (gCOSY), ^{1}H-^{1}H total correlation spectroscopy (TOCSY), and proton-detected ^{1}H-^{13}C-gradient-enhanced heteronuclear single quantum coherence (gHSQC) experiments were performed at 35°C on Varian Unity Inova, 500 MHz (Department of Chemistry, University of New Hampshire), 600 MHz, and 800 MHz (Complex Carbohydrate Research Center, University of Georgia) spectrometers, using standard acquisition software available in the Varian VNMR software package. Proton chemical shifts are referenced to internal tetramethylsilane (δ = 0.000 ppm). Carbon chemical shifts are referenced to solvent DMSO (δ = 40.0 ppm); because these were not obtained from directly detected 1-D spectra but were measured in F1 of the gHSQC experiment, values are given to single decimal place only.

Positive ion mode ESI-MS

Mass spectrometry was performed in the positive-ion mode on a Micromass Global (Manchester, UK) hybrid ESI-Qq/oa-TOF-MS instrument, with GIPC sample introduction via direct infusion in 100% MeOH (~100 ng/μl). The flow rate was usually 0.5 μl/min, but for analysis of An-5, which was available in limited amounts, a nano-spray capillary tip was employed, from which the flow rate was estimated to be ~200 nl/min. For generation of $[M(Li) + Li]^+$ adducts of GIPC molecular species, LiI (10 mM) in MeOH was added to the analyte solution until the observed ratio of $[M(Li) + Li]^+$ adducts to mixed Na^+/Li^+ adducts in MS profile mode was >5:1; the necessary LiI concentration was generally in the range of 3 to 5 mM. In general, spectra represent summations of 50–350 scans (30 scans/min) for MS $[M(Li) + Li]^+$ profiles and MS/CID-MS experiments. Resolution was generally 4,000 (5% valley) for MS profile spectra and 3,000 for MS/CID-MS experiments. Extraction cone voltage (analogous to orifice-to-skimmer potential in Sciex API series instruments) was 35 V for MS profile spectra and MS/CID-MS experiments, and 80 V for pseudo-$^+$ESI-(CID-MS)^2 experiments. Nominal, monoisotopic *m/z* values are used in the labeling and description of $^+$ESI-MS results. Interpretation of spectra derived from $[M(Li) + Li]^+$ adducts of GIPC molecular species was essentially as described previously (46).

Monosaccharide, inositol, fatty acid, and sphingoid component analysis by GC-MS

Monosaccharides were analyzed as their per-*O*-trimethylsilyl methyl glycosides. A re-*N*-acetylation step was used after methanolytic depolymerization to ensure that hexosamines, if present, would be detected as their acetamido derivatives. Ceramide-derived sphingoid bases and 2-hydroxy fatty acids were detected as their *N*-acetyl-per-*O*-trimethylsilyl and 2-*O*-trimethylsilyl methyl ester derivatives, respectively. All derivatives were prepared and analyzed by GC-MS according to protocols described previously (45). The instrument used was a GCQ (Finnigan MAT, San Jose, CA) operated in electron ionization (EI) mode. *Myo*-inositol was detected in the monosaccharide analysis as its per-*O*-trimethylsilyl derivative, although optimal conditions for its release (16) were not employed.

RESULTS

HPTLC profile and fractionation of *A. nidulans* GIPCs

Reproduced in **Fig. 1A** is an HPTLC of the crude acidic lipid fraction from *A. nidulans* A28 (37°C culture), stained with orcinol for detection of hexose-containing material (lane C), compared with a reference standard containing Manα3Manα2IPC and Gal*f*β6(Manα3)Manα2IPC (lane S). In general, such orcinol-stained bands in the acidic fraction of fungal lipids correspond to GIPCs. (IPC itself, having no carbohydrate content, is not detected by this method; on the other hand, hexose-containing impurities, including acidic oligosaccharides, may appear.) A similar profile, showing essentially three major (along with some minor) GIPC bands was obtained by Cheng et al. (35) from a different wild-type *A. nidulans* strain (A773) via [^{3}H]*myo*-inositol or [^{3}H]dihydrosphingosine metabolic precursor labeling and autoradiography. Note that the component with the highest R_f value comigrated with an authentic standard of Manα3Manα2IPC (M_2IPC) previously characterized from *Paracoccidioides brasiliensis* (45), but the most abundant component (middle band) had a significantly lower R_f than did the other major GIPC from *P. brasiliensis*, Gal*f*β6(Manα3)Manα2IPC (G_fM_2IPC). A third, less-abundant component migrated with a considerably lower R_f, consistent with attachment of one or two additional monosaccharide units. The crude lipids were fractionated by preparative-scale HPLC (Fig. 1B), with each of the three major components obtained in at least one fraction as a single orcinol-stained band (lanes 2, 4, and 6); these components, designated An-2, -3, and -5, respectively, were subjected to characterization by ^{1}H-NMR, MS, and GC-MS techniques as described below. An amount of An-3 sufficient for extensive 2-D NMR analysis was accumulated from three HPLC fractionations. An additional very minor component (An-4) could be detected (migrating between An-3 and An-5 in Fig. 1B, lane 5), but could not be purified sufficiently for individual characterization.

Monosaccharide, inositol, fatty acid, and sphingoid component analysis of *A. nidulans* GIPCs

Mannose was essentially the only monosaccharide identified by GC-MS analysis of the trimethylsilylated methyl glycosides produced following methanolysis of An-2, -3, and -5. *Myo*-inositol was also detected in all three fractions. The only long-chain fatty acid detected in significant amounts in all fractions was h24:0, identified by its characteristic retention time and fragments observed in its EI mass spectrum [as reviewed in ref. (47)]. A trace (<1%) of h25:0 fatty acid was detected in An-3. Traces (<2%) of nonhydroxy 16:0, 18:0, and 24:0 fatty acids were also detected in all fractions. No dihydroxy fatty acids were detected. The major sphingoid components detected were t18:0 and t20:0 4-hydroxysphinganines (phytosphingosines); the observed ratios were ~3:2 for An-2, ~2:3 for An-3, and ~3:2 for An-5. Under conditions of ion trap detection, EI spectra of the 4-hydroxysphinganine-derived *N*-acetyl-1,3,4-tri-*O*-trimethylsilyl-4-hydroxysphinganines were qualitatively similar in most respects to those published previously by Thorpe and Sweeley (48), but with more abundant representation of high-*m/z* ions, including some additional molecular mass-related ions as observed by Levery et al. (45). Thus, $[M - 15]^+$, $[M - 15 - 90]^+$, $[M - 59 - 90]^+$, $[M - 174]^+$, and $[M - 174 - 90]^+$ ions were observed at *m/z* 560, 470, 426, 401, and 311 for the t18:0 base derivative, and at *m/z* 588, 498, 454, 429, and 329 for the later-eluting t20:0 base derivative [data not shown; for detailed interpretations, including identifications of lower-*m/z* ions, see refs (48–50)].

^{1}H-NMR spectroscopic analysis of *A. nidulans* GIPCs

An-2. Parts of the ^{1}H-NMR spectrum of An-2 were obscured by resonances from a major orcinol-negative component. However, a pair of proton resonances was clearly observed in the anomeric region (**Fig. 2A**) at 4.896 ppm

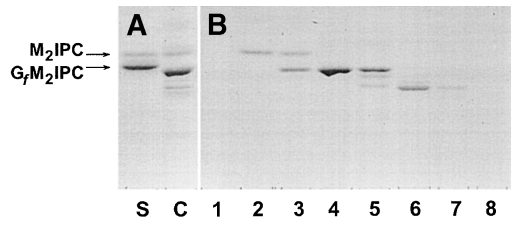

Fig. 1. High-performance thin-layer chromatography (HPTLC) analysis (orcinol stain) of glycosylinositol phosphorylceramides (GIPCs) from *A. nidulans*. Mobile phase, chloroform-methanol-water (50:47:14; v/v/v, containing 0.038% w/v $CaCl_2$). A: Lane S, GIPC standard containing Manα1→3Manα1→2Ins1-P-1Cer (M_2IPC) and Manα1→3(Gal*f*β1→6)Manα1→2Ins1-P-1Cer (G_fM_2IPC); Lane C, crude acidic fraction from *A. nidulans*. B: Lanes 1–8, consecutive fractions 18–25 from HPLC of crude *A. nidulans* acidic lipids (40 × 2 ml fractions collected at 0.5 ml/min).

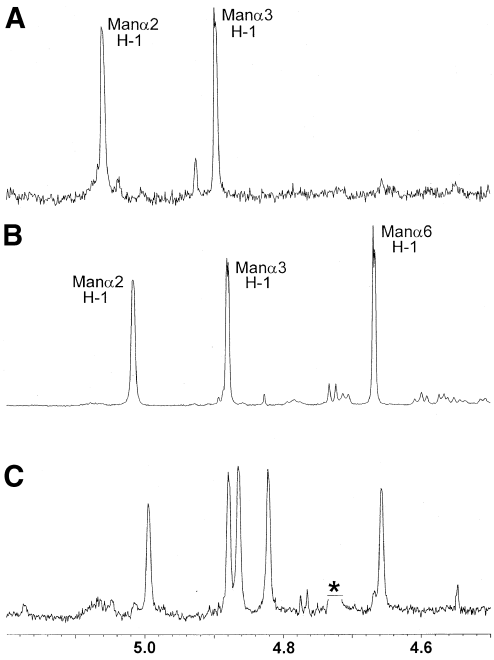

Fig. 2. Downfield expansions (5.20–4.50 ppm) of 1-D ^{1}H-NMR spectra (800 MHz; DMSO-d_6/2% D_2O; 35°C) of GIPC fractions isolated from *A. nidulans*; spectra were acquired on fractions corresponding to lanes 2, 4, and 6 shown in Fig. 1B. A: An-2 (lane 2); B, An-3 (lane 4); C: An-5 (lane 6).

($^3J_{1,2}$ = 1.5 Hz) and 5.059 ppm ($^3J_{1,2}$ < 2.0 Hz); these chemical shift values are essentially identical to those found previously for H-1 of the Manα3 and Manα2 residues, respectively, of Manα3Manα2IPC from *P. brasiliensis* (45). This GIPC has been obtained from a variety of fungi (45) (S. B. Levery, M. S. Toledo, A. H. Straus, and H. K. Takahashi, unpublished observations) and is easily recognizable by its anomeric proton signature and HPTLC R_f identical to that of a fully characterized Manα3Manα2-IPC. Therefore, this fraction was considered to be identified by adequate criteria and was not purified or characterized further.

An-3. The 1-D ^{1}H-NMR spectrum of fraction An-3 (**Fig. 3A**) showed it to be a nearly homogeneous GIPC component, displaying only a few minor impurity peaks. As shown in detail in Fig. 2B, three anomeric proton resonances are clearly observed in the spectrum at 4.666 ppm ($^3J_{1,2}$ = 1.4 Hz), 4.877 ppm ($^3J_{1,2}$ = 1.5 Hz), and 5.013 ppm ($^3J_{1,2}$ = 1.5 Hz). All three of the $^3J_{1,2}$ values are consistent with α-Man*p*, although the resonance at 4.666 ppm appears rather upfield (under these conditions) compared with the H-1 signals of other GIPC α-Man residues we have encountered. However, ample precedent for this large upfield decrement can be found in NMR spectroscopy (in D_2O) of high-mannose glycoprotein *N*-glycans, where H-1 of nonreducing terminal Manα1→6 residues are observed at 0.18–0.22 ppm upfield from H-1 of terminal Manα1→3 (51, 52). Almost all monosaccharide, inositol, and ceramide resonances were unambiguously assignable from 2-D ^{1}H-^{1}H gCOSY and TOCSY experiments (Fig. 3B, C and **Table 1**). Analysis of approximate $^3J_{i,j}$ proton coupling constants around the three monosaccharide spin systems confirmed their identities as α-Man*p* residues. Analysis of approximate $^3J_{i,j}$ coupling constants around the cyclic Ins spin system confirmed it as *myo*-inositol (all hydroxyl groups equatorial except that at C-2), while the chemical shift pattern, compared with previously acquired data, was consistent with glycosylation of Ins at O-2 (45, 53–55). In the nuclear Overhauser effect (NOE) spectroscopy spectrum (Fig. 3D), a strong NOE cross-peak is observed between the α-Man*p* H-1 at 5.013 ppm and Ins H-2 at 3.954 ppm (resolvable despite partial overlap with the expected intraresidue α-Man*p* H-1/H-2 cross-peak at 3.939 ppm), thus correlating the partners in a Manα1→2Ins core linkage. The linkage of the other two α-Man*p* residues to the first at O-3 and O-6 is supported by strong NOE cross-peaks correlating the H-1 resonating at 4.877 ppm with H-3 of Manα2 at 3.620 ppm (in addition to weaker correlations with H-2 and H-4 of that residue) and the H-1 resonating at 4.666 ppm with H-6a of Manα2

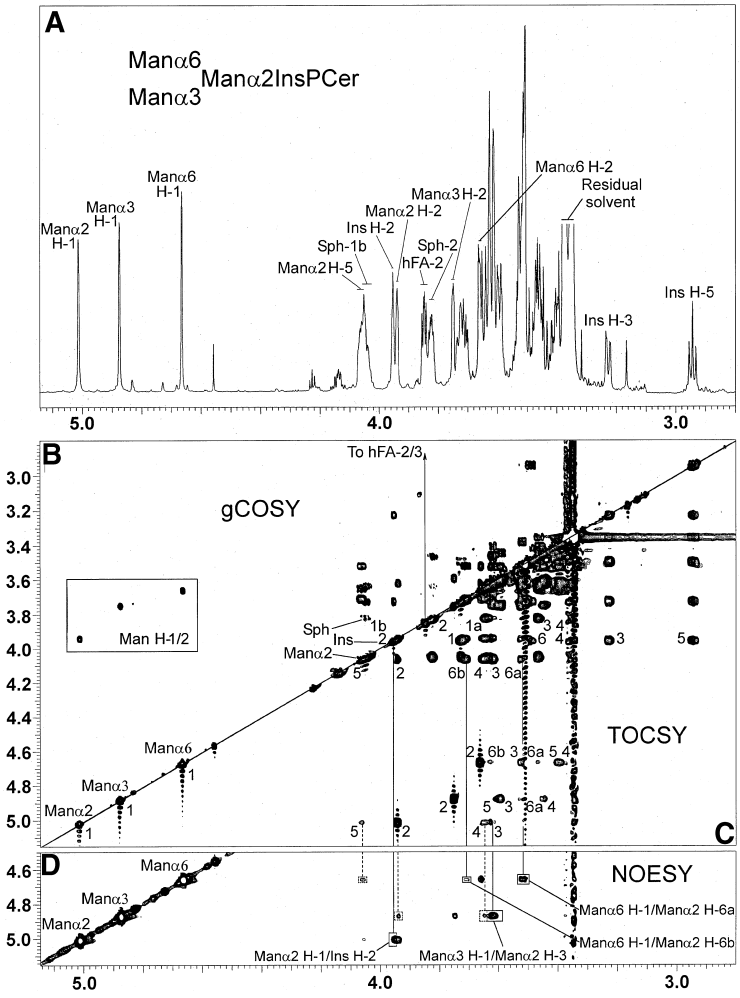

Fig. 3. Downfield expansions (5.15–2.80 ppm) of one-dimensional (1-D) and 2-D ^{1}H-NMR spectra (800 MHz; DMSO-d_6/2% D_2O; 35°C) of *A. nidulans* GIPC fraction An-3 (combined yield from 3 HPLC purifications). A: 1-D spectrum. B: Upper left section of 2-D ^{1}H-^{1}H g correlation spectroscopy spectrum. C: Lower right section of 2-D ^{1}H-^{1}H total correlation spectroscopy spectrum (200 msec mixing time). D: 2-D ^{1}H-^{1}H nuclear Overhauser effect spectroscopy spectrum (100 msec mixing time; F_1, 5.1–4.5 ppm). In D, inter-residue nuclear Overhauser effect correlations across glycosidic linkages are boxed; weaker nonglycosidic inter-residue correlations are marked by dashed boxes; intraresidue correlations have been left unmarked.

TABLE 1. ^{1}H and ^{13}C chemical shifts (ppm) for monosaccharide, inositol, ceramide sphingoid, and fatty-*N*-acyl (in parentheses) residues of Manα6(Manα3)Manα2IPC (An-3) from *A. nidulans* in DMSO-d_6/2% D_2O at 35°C

An-3	Manα1→6	(Manα1→3)	Manα1→2	Ins1→P→1	Cer
H-1	4.666	4.877	5.013	3.728	3.640, 4.050
($^{3}J_{1,2}$)	(1.4)	(1.5)	(1.5)		
H-2	3.659	3.749	3.939	3.954	3.824 (3.848)
H-3	3.520	3.592	3.620	3.228	3.467
H-4	3.383	3.448	3.650	3.360	3.357
H-5	3.410	3.588	4.060	2.942	
H-6	3.462	3.540	3.520	3.492	
H-6′	3.622	3.608	3.703		
C-1	99.9	102.2	101.0	76.0	64.3
C-2	70.2	70.5	69.5	77.8	50.3 (71.3)
C-3	70.9	70.9	79.1	70.6	72.8
C-4	67.0	67.1	64.6	72.4	70.3
C-5	73.7	73.5	71.5	75.6	
C-6	61.3	61.1	65.3	72.6	

Ins, *myo*-inositol; Cer, ceramide. $^{3}J_{1,2}$ (Hz) for monosaccharide residues are given in parentheses.

at 3.520 ppm (in addition to weaker correlations with H-6b and H-5 of that residue). Although severe spectral overlap renders the interglycosidic Manα6 H-1/Manα2 H-6a correlation somewhat ambiguous by itself (other protons resonate at or near 3.520 ppm), the additional Manα6 H-1/Manα2 H-6b and Manα6 H-1/Manα2 H-5 correlations, though weak, are observed at nondegenerate monosaccharide proton frequencies (3.703 ppm and 4.060 ppm, respectively), and merely incidental appearance of these without that relating Manα6 H-1 with Manα2 H-6a is highly unlikely. Interestingly, the extreme downfield shift of H-5 was observed previously in a GIPC having the Manα2 residue substituted at O-3 and O-6, i.e., in the case of Gal*f*β6(Manα3)Manα2IPC from *P. brasiliensis* (45).

Finally, ^{13}C resonance assignments (Table 1), made from a 2-D ^{1}H-detected, ^{13}C-^{1}H gHSQC spectrum (not shown), were also consistent with the linkage of two of the α-Man*p* residues to the core Manα2 residue at O-3 and O-6; this is supported by a pattern of substantial downfield shift increments (α-effects) for Manα2 C-3 and C-6, along with upfield shift decrements (β-effects) (56) for Manα2 C-2, C-4, and C-5, compared with ^{13}C spectral data for the parent compound, Manα2IPC (54). All other ^{13}C chemical shifts are consistent with the proposed Manα2IPC core structure, including those characteristic of the *myo*-Ins residue substituted at O-2 (54). On the basis of all of these data, the structure of An-3 was proposed to be Manα6(Manα3)Manα2IPC.

Further confirmation of the structure of An-3 was obtained by comparison of its NMR spectrum with that of an authentic sample of Manα6(Manα3)Manα2IPC ("Cc-2") previously found in a Basidiomycete species, *Cantharellus cibarius* (Chantarelle) (55). As shown in **Fig. 4**, the NMR spectrum of *C. cibarius* Cc-2 is almost identical to that of An-3 except for some doubling of the Ins-5 resonance, a spectral feature that appears to be associated in general with the presence of a second ceramide type containing dihydroxy-fatty-*N*-acylation (S. B. Levery, unpublished observations), already known to be present in the *C. cibarius* GIPC preparation (55). In particular, the three monosaccharide H-1 signals are observed at identical chemical shifts, each with the same $^{3}J_{1,2}$ coupling constant as found for An-3. Because the branched Manα6(Manα3)Manα structure was confirmed unambiguously for Cc-2 by methylation linkage analysis (55), the structure of An-3 is thereby confirmed as well.

An-5. The third GIPC fraction, An-5, yielded a very complex ^{1}H-NMR spectrum, and too little material was available for extensive application of 2-D NMR analysis; however, five signals with similar intensity and line width ($^{3}J_{1,2}$ <2.0 Hz) are clearly observable in the H-1 region of the 1-D spectrum at 4.994, 4.878, 4.864, 4.821, and 4.657 ppm (Fig. 2C), and each of their correlated H-2 partners was assignable (**Table 2**) from correlations observed in an otherwise poor-quality TOCSY spectrum (not shown). Three of the H-1 signals occur at chemical shifts near those of the anomeric protons in An-3, suggesting a structure for An-5 based on elaboration of the Manα6(Manα3)Manα2IPC core, with two additional α-Man residues. Even provisional assignment for the linkages of the two additional residues based on these data is problematic; however, a number of

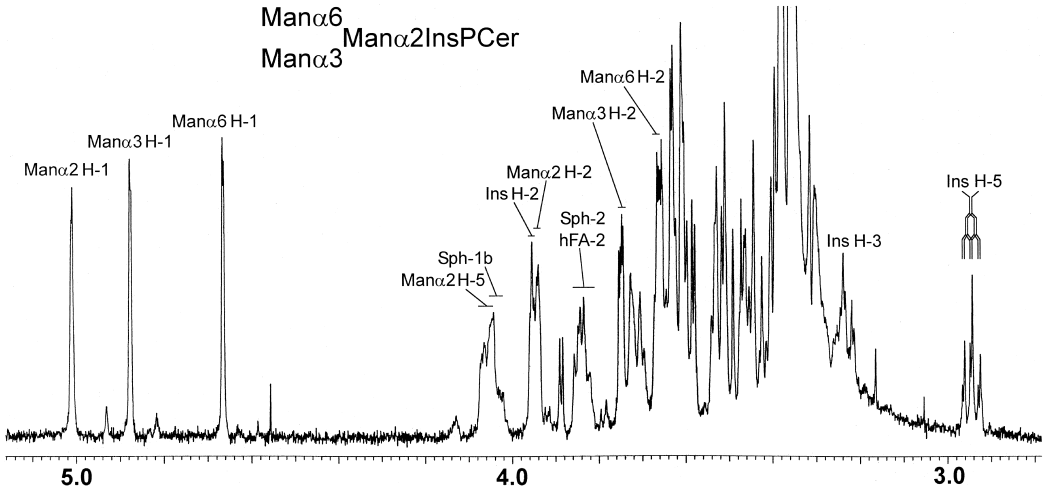

Fig. 4. Downfield expansion (5.15–2.80 ppm) of 1-D ^{1}H-NMR spectrum (500 MHz; DMSO-d_6/2% D_2O; 35°C) of *C. cibarius* GIPC fraction Cc-2.

TABLE 2. Proposed structure and ^{1}H chemical shifts (ppm) for H-1 and H-2 of monosaccharide residues of An-5 from *A. nidulans* in DMSO-d_6/2% D_2O at 35°C

An-5	Manα1→2	Manα1→6	Manα1[a]→6	(Manα1→3)	Manα1→2	InsPCer
H-1	4.864[b]	4.821[b]	4.657	4.878[b]	4.994	
($^3J_{1,2}$)	(<2.0)	(<2.0)	(<2.0)	(<2.0)	(<2.0)	
H-2	3.726[b]	3.698[b]	3.677	3.766[b]	3.953	

$^3J_{1,2}$ (Hz) for monosaccharide residues are given in parentheses.

[a] The nonreducing terminal disaccharide is proposed to be linked to the branching Manα6 rather than the Manα3 residue, but this has not been unambiguously determined.

[b] Among these Manα residues, assignments of H-1/H-2 pairs may be interchanged.

arguments can be made to narrow the field of likely structures for An-5.

First, assignment of the H-1 resonance at 4.994 ppm to the core branching Manα2 residue is supported by observation of its correlated H-2 signal at 3.953 ppm, close to the value observed for this proton in An-3 (3.939 ppm). This is a significant point, inasmuch as this relatively downfield-shifted value for α-Man H-2 is characteristic for glycosylation of this residue at O-3, e.g., by a second α-Man residue, compared with unglycosylated (terminal) α-Man; by contrast, the effects of glycosylation of α-Man at O-6, and even O-2, on this resonance are relatively negligible (51, 52). Analysis of NMR data on GIPCs acquired under similar conditions (45, 53, 54), including the data for An-3 in this work, shows that H-2 of the penultimate residue in a Manα3Manα disaccharide can be found in the range 3.88–4.08 ppm (5 cases), compared with 3.66–3.77 ppm for a terminal α-Man residue (7 cases). Thus, barring unexpected conformational effects, the lack of significant downfield shifts for H-2 of the four remaining α-Man residues of An-5 (all in the range of 3.67–3.77 ppm) (Table 2) tends to preclude glycosylation at O-3; i.e., neither of the two Man residues added onto the An-3 core is in an α1→3 linkage. Second, we propose that glycosylations at O-4 can be excluded (at least provisionally), based on the lack of reports of structures containing a Manα4Man disaccharide, or of α-mannosyltransferases able to make this linkage. The two additional Man residues are therefore likely to be linked either α1→2 or α1→6.

The field of possible structures can be further narrowed by consideration of the cumulative effects of adding Man residues, in either α1→2 or α1→6 linkage, on the H-1 subspectrum of An-3, taking into account what is already known of these effects from "structure reporter group" analysis of many closely related oligo-α-mannose-type glycans (51, 52). For example, all structures one could propose involving addition of both residues in α1→6 linkage are excluded, because one would then expect to find three H-1 resonances in the upfield region around 3.66–4.67 ppm. One possible structure for An-5, consistent with the available NMR data, would be addition of a Manα2Manα6 disaccharide to the Manα6 residue of An-3. Considering the effects one at a time, addition of the second Manα6 residue could be responsible for a slight upfield shift of H-1 of the first (from 4.666 ppm in An-3 to 4.657 ppm observed in An-5), but would itself be expected to give rise to a second H-1 resonance in the same region of the spectrum. However, subsequent addition of a Manα2 residue would then be expected to cause a significant downfield shift for H-1 of this second Manα6 residue (observed at 4.821 ppm in An-5). Another possibility, consistent with the same reasoning, is addition of the Manα2 residue to the inner Manα6 to create a doubly branched Manα6(Manα2)Manα6(Manα3)Manα structure. However, mass spectrometric analysis (see subsequent section) appears more consistent with a single linear branch as proposed above, and tended to exclude as well structures formed by extension of both the Manα6 and Manα3 residues of An-3 by one additional monosaccharide. Other "soft" criteria may allow one at least to make some provisional judgments. For example, addition of the same sugars in reverse order (Manα6Manα2) is not categorically excluded by the NMR data but seems less likely, based on analogy to known oligo-α-mannose structures. Finally, the possibility that the disaccharide extension has been added to the Manα3 residue of An-3 can be considered less likely, because the resonance appearing in the spectrum of An-3 at 4.877 ppm, assigned as H-1 of the Manα3 residue, also appears in the spectrum of An-5 virtually unshifted at 4.878 ppm. However, it is also possible that this Manα3 H-1 resonance has indeed been shifted upfield (e.g., to 4.864 ppm by Manα6 glycosylation), while the H-1 of one of the additional residues coincidentally resonates at the same chemical shift in An-5; therefore, this alternative structure is not definitively excluded.

$^+$ESI-MS and MS/CID-MS analysis of *A. nidulans* GIPCs

An-3. A molecular profile of GIPC fraction An-3 was acquired via $^+$ESI-Q/oa-TOF-MS (**Fig. 5A**); a pair of $[M(Na) + Na]^+$ salt adduct ions observed at *m/z* 1,456 and 1,484 is consistent with an M_3IPC having ceramides consisting of t18:0/t20:0 4-hydroxysphinganines with h24:0 fatty-*N*-acylation. Less-abundant ions at *m/z* 1,472 and 1,500 represent the same molecular species with single substitutions of K^+ for Na^+ (see below). Addition of LiI shifted the profile to predominant $[M(Li) + Li]^+$ adducts at *m/z* 1,424 and 1,452, with residual mixed Na^+/Li^+ adducts present at lower abundance at *m/z* 1,440 and 1,468 (Fig. 5B). The latter ions could in principle represent molecular components containing dihydroxy-fatty-*N*-acylation, because this modification would also increment by 16 the *m/z* values of the predominant components. However, dihydroxy fatty acids were not detected in the component analysis.

In general, $^+$ESI-MS/CID-MS spectra acquired [via $^+$ESI-Q/q(CID)-oa-TOF-MS] from either disodiated or dilithiated molecular adducts exhibited abundant pairs of fragment ions representing the complete glycosylinositol $\{[B_3 + cation\ (Cat)]^+$ and $(C_3 + Cat)^+\}$ and glycosylinositol phosphate $\{[B_3PO_3(Cat) + Cat]^+$ and $[C_3PO_3(Cat) + Cat]^+\}$ moieties, along with ceramide ($[Y_0 + Cat]^+$ and $[Z_0 + Cat]^+$) and ceramide phosphate $\{[Y_0PO_3(Cat) + Cat]^+$ and $[Z_0PO_3(Cat) + Cat]^+\}$ ions (see **Scheme 2**). Ions in parallel series, representing glycosidic fragmentations occurring singly or in combination with other cleavages (the

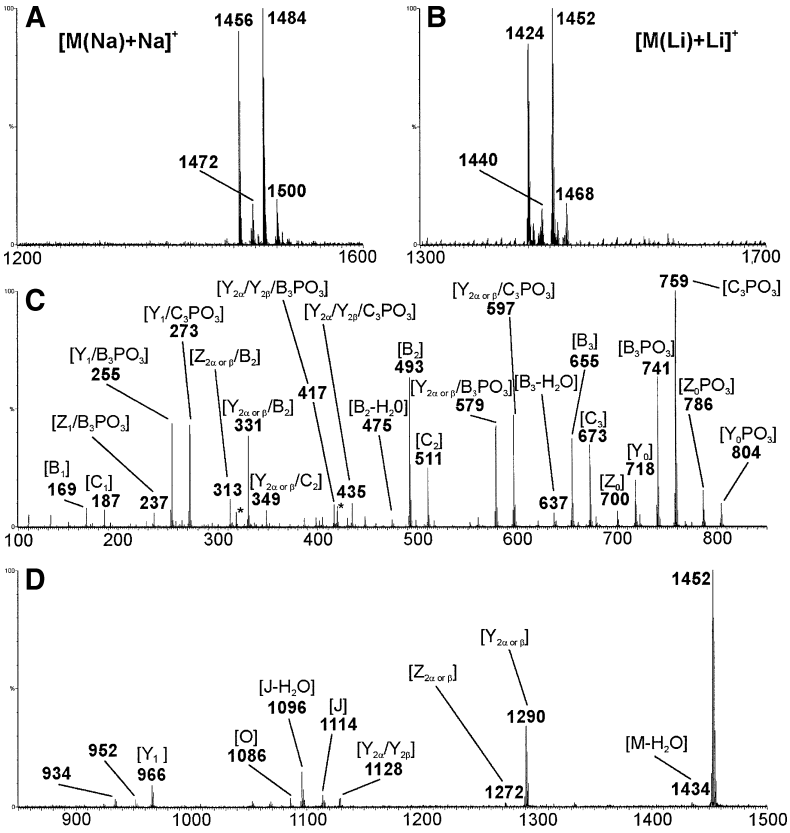

Fig. 5. $^{+}$ESI-hybrid quadrupole/time-of-flight (Qq/oa-TOF) spectra of An-3. A: Profile of molecular ions as $[M(Na) + Na]^{+}$ adducts. B: Profile of molecular ions as $[M(Li) + Li]^{+}$ adducts. C: Mass spectrometry/collision-induced dissociation-mass spectrometry (MS/CID-MS) of $[M(Li) + Li]^{+}$ at *m/z* 1,452, low *m/z* region. D: MS/CID-MS of $[M(Li) + Li]^{+}$ at *m/z* 1,452, high *m/z* region. The Y-axis expansion in D relative to C is 27×. Ion designations correspond to Scheme 3. The designations "+Li" and "(Li) + Li" and the charge form have been omitted from the fragment labels for clarity.

latter denoted by one or more "/"), were also observed {$[C_n + Cat]^{+}$, $[B_n + Cat]^{+}$, $[Y_n + Cat]^{+}$, $[Z_n + Cat]^{+}$, $[Y_m/C_n + Cat]^{+}$, $[Y_m/B_n + Cat]^{+}$, $[Y_m/C_nPO_3(Cat) + Cat]^{+}$, and $[Y_m/B_nPO_3(Cat) + Cat]^{+}$}. In many cases, $[Z_m/B_nPO_3(Cat) + Cat]^{+}$ and $[Z_m/B_n + Cat]^{+}$ ions were also observed. Of these fragments, the $[Y_m/C_nPO_3(Cat) + Cat]^{+}$ and $[Y_m/B_nPO_3(Cat) + Cat]^{+}$ series were the most useful for deducing glycosidic sequence, because the presence of the phosphate moiety clearly labels the inositol-containing reducing end of the glycan. $^{+}$ESI-MS/CID-MS of $[M(Li) + Li]^{+}$ adducts yielded better overall *S/N* than $[M(Na) + Na]^{+}$ adducts, although the differences were not as pronounced as previously reported with the use of a triple quadrupole for $^{+}$ESI-MS/CID-MS analysis of GIPCs (46).

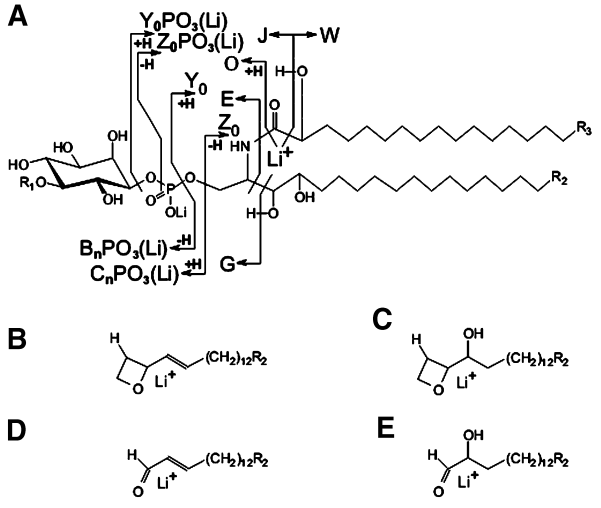

Scheme 2. Characteristic fragmentations of glycosylated IPCs. A: Nomenclature of Adams and Ann (73) for fragmentation of the ceramide moiety, and of Singh, Costello, and Beach (74) for the *myo*-inositol phosphoryl group. B: Sphingoid $\underline{d}_{3b}$ ion, proposed by Hsu and Turk (57). C: Hydrated analog of $\underline{d}_{3b}$ ion, proposed in this study as a product of t18:0 or t20:0 phytosphingosine-containing ceramides. D: Sphingoid $\underline{c}_{1b}$ ion, proposed by Hsu and Turk (57). E: Hydrated analog of $\underline{c}_{1b}$ ion, proposed in this study as a product of t18:0 or t20:0 phytosphingosine-containing ceramides.

An $^{+}$ESI-MS/CID-MS spectrum acquired from the dilithiated molecular adduct at *m/z* 1,452 is reproduced in Fig. 5C, D, showing the predominant $[B_3PO_3(Li) + Li]^{+}/[C_3PO_3(Li) + Li]^{+}$ pair (*m/z* 741/759) and other abundant fragments (summarized in **Table 3**). Consistent with previous findings (45, 46), a somewhat lower abundance is observed for glycosylinositol phosphate fragment ions requiring at least two glycosidic cleavages for their appearance {$[Y_{2\alpha}/Y_{2\beta}/B_3PO_3(Li) + Li]^{+}$ and $[Y_{2\alpha}/Y_{2\beta}/C_3PO_3(Li) + Li]^{+}$, at *m/z* 417 and 435, respectively}, compared with other ions in the $[Y_m/B_nPO_3(Li) + Li]^{+}$ and $[Y_m/C_nPO_3(Li) + Li]^{+}$ series, indicating the presence of a branch point in the glycan (see **Scheme 3**). In particular, the ratios of the relative abundances of *m/z* 435 versus *m/z* 273 (0.22), and *m/z* 435 versus *m/z* 597 (0.16), are attenuated by a factor of 3 in An-3 when compared with the same ratios in an isomeric unbranched triglycosyl GIPC structure (0.70 and 0.52, respectively) (B. Bennion, S. B. Levery, M. S. Toledo, A. H. Straus, and H. K. Takahashi, unpublished observations). Such differences in abundance ratios appear to be typical under these conditions.

TABLE 3. Glycosylinositol- and phosphorylglycosylinositol-related product ions formed in low-energy ESI-MS/CID-TOF-MS spectra of tri- and pentamannosylinositol phosphorylceramides from mycelia of *A. nidulans*

m/z	An-3a,b	An-5a,b
1,083		**$[C_5PO_3(Li) + Li]^+$**
1,065		$[B_5PO_3(Li) + Li]^+$
1,047		$[B_5PO_3(Li) + Li - H_2O]^+$
997		$[C_5 + Li]^+$
979		$[B_5 + Li]^+$
921		$[Y_{4\alpha \text{ or } 2\beta}/C_5PO_3(Li) + Li]^+$
903		$[Y_{4\alpha \text{ or } 2\beta}/B_5PO_3(Li) + Li]^+$
835		$[Y_{4\alpha \text{ or } 2\beta}/C_5 + Li]^+$ or $[C_4 + Li]^+$
817		$[Y_{4\alpha \text{ or } 2\beta}/B_5 + Li]^+$ or $[B_4 + Li]^+$
759	**$[C_3PO_3(Li) + Li]^+$**	$[Y_{3\alpha}/C_5PO_3(Li) + Li]^+$
741	$[B_3PO_3(Li) + Li]^+$	$[Y_{3\alpha}/B_5PO_3(Li) + Li]^+$
723	$[B_3PO_3(Li) + Li - H_2O]^+$	$[Z_{3\alpha}/B_5PO_3(Li) + Li]^+$
673	$[C_3 + Li]^+$	$[Y_{3\alpha}/C_5 + Li]^+$ or $[Y_{4\alpha}/C_4 + Li]^+$
655	$[B_3 + Li]^+$	$[Y_{3\alpha}/B_5 + Li]^+$ or $[Z_{3\alpha}/C_5 + Li]^+$ [a]
637	$[B_3 + Li - H_2O]^+$	$[Z_{3\alpha}/B_5 + Li]^+$ or $[Z_{4\alpha}/B_4 + Li]^+$
597	$[Y_{2\alpha \text{ or } \beta}/C_3PO_3(Li) + Li]^+$	$[Y_{2\alpha}/C_5PO_3(Li) + Li]^+$
579	$[Y_{2\alpha \text{ or } \beta}/B_3PO_3(Li) + Li]^+$	$[Y_{2\alpha}/B_5PO_3(Li) + Li]^+$
561	$[Z_{2\alpha \text{ or } \beta}/B_3PO_3(Li) + Li]^+$	$[Z_{2\alpha}/B_5PO_3(Li) + Li]^+$
511	$[Y_{2\alpha \text{ or } \beta}/C_3 + Li]^+$ or $[C_2 + Li]^+$	$[Y_{2\alpha}/C_5 + Li]^+$ or $[C_3 + Li]^+$
493	$[Y_{2\alpha \text{ or } \beta}/B_3 + Li]^+$ or $[B_2 + Li]^+$	$[Y_{2\alpha}/B_5 + Li]^+$ or $[Z_{2\alpha}/C_5 + Li]^+$ or $[B_{3\alpha} + Li]^+$ [b]
475	$[Z_{2\alpha \text{ or } \beta}/B_3 + Li]^+$ or $[B_2 + Li - H_2O]^+$	$[Z_{2\alpha}/B_5 + Li]^+$ or $[B_{3\alpha} + Li - H_2O]^+$
435	$[Y_{2\alpha}/Y_{2\beta}/C_3PO_3(Li) + Li]^+$	$[Y_{2\alpha}/Y_{2\beta}/C_5PO_3(Li) + Li]^+$
417	$[Y_{2\alpha}/Y_{2\beta}/B_3PO_3(Li) + Li]^+$	$[Y_{2\alpha}/Y_{2\beta}/B_5PO_3(Li) + Li]^+$
349	$[Y_{2\alpha \text{ or } \beta}/C_2 + Li]^+$	$[C_{2\alpha} + Li]^+$
331	$[Y_{2\alpha \text{ or } \beta}/B_2 + Li]^+$ or $[Z_{2\alpha \text{ or } \beta}/C_2 + Li]^+$	$[B_{2\alpha} + Li]^+$
313	$[Z_{2\alpha \text{ or } \beta}/B_2 + Li]^+$	$[B_{2\alpha} + Li - H_2O]^+$
273	$[Y_1/C_3PO_3(Li) + Li]^+$	$[Y_1/C_5PO_3(Li) + Li]^+$
255	$[Y_1/B_3PO_3(Li) + Li]^+$	$[Y_1/B_5PO_3(Li) + Li]^+$
237	$[Z_1/B_3PO_3(Li) + Li]^+$	$[Z_1/B_5PO_3(Li) + Li]^+$
187	$[Y_1/C_3 + Li]^+$ or $[C_{1\alpha \text{ or } \beta} + Li]^+$	$[C_{1\alpha \text{ or } \beta} + Li]^+$
169	$[Y_1/B_3 + Li]^+$ or $[B_{1\alpha \text{ or } \beta} + Li]^+$	$[B_{1\alpha \text{ or } \beta} + Li]^+$
111	$[LiH_2PO_4 + Li]^+$	$[LiH_2PO_4 + Li]^+$

ESI-MS/CID-TOF-MS, electrospray ionization-mass spectrometry/collision-induced decomposition-time-of-flight-mass spectrometry. Base peak is distinguished by bold font. Fragment designations are as in Costello and Vath (75), as expanded for glycosylinositol phosphorylceramides (GIPCs) in Singh, Costello, and Beach (74), illustrated in Schemes 3–5.

[a] Or $[Y_{4\alpha}/B_4 + Li]^+$ or $[Z_{4\alpha}/C_4 + Li]^+$.

[b] Or $[Y_{3\alpha}/B_4 + Li]^+$ or $[Z_{3\alpha}/C_4 + Li]^+$.

In addition to glycosidic fragment series derived from the glycosylinositol phosphate and glycosylinositol moieties, fragments from sequential loss of monosaccharide residues from $[M(Li) + Li]^+$ $\{[Y_m(Li) + Li]^+\}$, which were not observed significantly in previous $^+$ESI-MS/CID-MS of GIPCs acquired on a triple-quadrupole instrument (45, 46), appear at lower abundance in the $^+$ESI-Q/q(CID)-oa-TOF-MS (Fig. 5D, **Table 4**). In the same region of the spectra and at similar abundance, ions from loss of the acyl chain and loss of acyl C_2-C_ω $\{[O(Li) + Li]^+$, $[J(Li) + Li]^+$, and $[J(Li) + Li - H_2O]^+\}$ are also observed. Within this group, the latter ion appears to be predominant. Similar to previous results (46), the ceramide and ceramide phosphate ions $\{[Y_0 + Li]^+$, $[Z_0 + Li]^+$, $[Y_0PO_3(Li) + Li]^+$, and $[Z_0PO_3(Li) + Li]^+\}$ appear at intermediate abundances; in addition, ions corresponding to $[O/Z_0PO_3(Li) + Li]^+$ and a hydrated $\underline{d}_{3b}$ analog (see Scheme 2C) are observed at lower abundances (*m/z* 420 and 319, respectively, denoted by asterisks in Fig. 5C). An essentially identical spectrum, except for those ions containing all or part of the ceramide moiety, was obtained via $^+$ESI-MS/CID-MS of the molecular adduct at *m/z* 1,424 (not shown); in this case all ions containing the ceramide or sphingoid were decremented by *m/z* 28 (see Table 4). The $[O(Li) + Li]^+$, $[J(Li) + Li]^+$, $[J(Li) + Li - H_2O)]^+$, and $[O/Z_0PO_3(Li) + Li]^+$ ions all provide information about the carbon number of the sphingoid and, by difference, the *N*-acyl chain, all or part of which is lost in the process of their formation. In this case, in agreement with the sphingoid and fatty acid analysis, they indicate that the *m/z* 28 increment between the two predominant molecular species is primarily due to a corresponding C_2H_4 difference in the sphingoid rather than the *N*-acyl chain. Thus the $[M(Li) + Li]^+$ adducts at *m/z* 1,424 and 1,452 correspond to molecular species containing t18:0 and t20:0 4-hydroxysphinganines with h24:0 fatty-*N*-acylation.

This was further confirmed by pseudo-$^+$ESI-(CID-MS)^2 experiments, using a high extraction cone voltage (analogous to high orifice-to-skimmer potential in Sciex API™ series instruments) to generate in-source CID primary fragments [$^+$ESI-(CID)], which are then selected by the first analyzer (Q) for subsequent generation of /q(CID)-oa-TOF product ion spectra (altogether, $^+$ESI-[CID]Q/q[CID]oa-TOF-MS). We and others (46, 53, 57) previously applied this technique to analysis of underivatized GSLs on a triple-quadrupole instrument. The most abundant

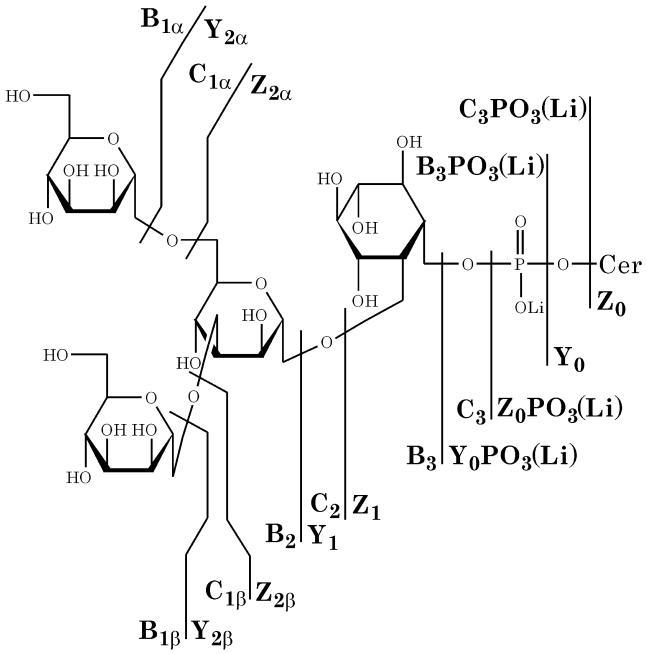

Scheme 3. Fragmentation of GIPC An-3 in positive-ion electrospray ionization-quadrupole/time-of-flight-mass spectrometry (ESI-Qq/oa-TOF-MS); ion designations according to Costello and Vath (75), and Singh, Costello, and Beach (74). The adduct designation "+Li" and the charge form have been omitted from the labels for clarity.

fragments in a high extraction cone voltage $^{+}$ESI-(CID)-Q/oa-TOF-MS profile of An-3 (not shown) were ceramide ions $[Y_0 + Li]^+$ (*m/z* 718 and 690) and the pair of glycosylinositol phosphate ions $[B_3PO_3(Li) + Li]^+/[C_3PO_3(Li) + Li]^+$ (*m/z* 759 and 741, respectively). Product ion spectra generated subsequently via $^{+}$ESI-(CID)-Q/q(CID)-oa-TOF-MS from the primary ions at *m/z* 718 and 690 are reproduced in **Fig. 6A** and Fig. 6B, respectively. These display abundant fragments corresponding to loss of the acyl chain ($[N + Li]^+ \equiv [O/Y_0 + Li]^+$) and a sphingoid rearrangement including additional loss of the amino group ($\underline{d}_{3b}$; see Scheme 2C). The $[N + Li]^+$ and $\underline{d}_{3b}$ ions are observed at *m/z* 352 and 319, respectively, in the spectrum of products from *m/z* 718, and at *m/z* 324 and 291, respectively, in the spectrum from *m/z* 690, confirming that the *m/z* 28 differences in the ceramide moieties reside entirely in the sphingoid chain lengths, while the *N*-acyl group is h24:0 in both ceramide species. Minor products included ions derived from these by dehydration or further fragmentation (Table 4). Ions derived from loss of all or most of the sphingoid alkyl chain, while retaining the fatty-*N*-acyl chain (e.g., $[S + Li]^+ \equiv [G/Y_0 + Li - H_2]^+$, $[T + Li]^+ \equiv [G/Z_0 + Li]^+$, $[U + Li]^+ \equiv [T + Li - C_2H_2]^+$) as well as an aldehyde ion derived from the fatty-*N*-acyl C_2-C_ω ($[W + Li]^+$), are observed at the same *m/z* in both spectra (see Table 4 and Scheme 2). The results are similar to those previously obtained with a triple-quadrupole spectrometer (46), but these spectra are of much higher quality.

An-5. A molecular adduct profile of GIPC An-5 (**Fig. 7A**) was consistent with a pentahexosyl-IPC structure as proposed, i.e., An-3 elaborated with two additional Man residues. In this case, the $^{+}$ESI-Q/oa-TOF-MS profile consisted of a pair of $[M(K) + K]^+$ adduct ions (*m/z* 1,812 and 1,840), accompanied by a slightly more abundant second pair of ions *m/z* 16 lower (*m/z* 1,796 and 1,824), representing the same molecular species with single substitutions of Na^+ for K^+, and a third pair *m/z* 32 lower (*m/z* 1,780 and 1,808), representing $[M(Na) + Na]^+$ adducts. Addition of LiI effectively consolidated the molecular profile into a pair of $[M(Li) + Li]^+$ adducts at *m/z* 1,748 and 1,776 (Fig. 7B). $^{+}$ESI-MS/CID-MS spectra acquired via $^{+}$ESI-Q/q(CID)-oa-TOF-MS on these $[M(Li) + Li]^+$ adducts both exhibited abundant fragment ion pairs at *m/z* 1,065 and 1,083 {designated $[B_5PO_3(Li) + Li]^+/[C_5PO_3(Li) + Li]^+$ or $[B_6PO_3(Li) + Li]^+/[C_6PO_3(Li) + Li]^+$, depending on whether the structure contains a branch

TABLE 4. Molecular adduct ions $[M(Li) + Li]^+$ observed in ESI-Q/TOF-MS profile (A), and significant ceramide-containing (B), sphingoid-containing and sphingoid-derived (C, D), and fatty-*N*-acyl-derived (E) product ions (*m/z*) formed in low-energy ESI-MS/CID-TOF-MS and ESI-CID-MS/CID-TOF-MS spectra of tri- and pentamannosylinositol phosphorylceramides from mycelia of *A. nidulans*

Fraction	An-3a	An-3b	An-5a	An-5b
Fatty acid	h24:0	h24:0	h24:0	h24:0
Sphingoid	t18:0	t20:0	t18:0	t20:0
A. $[M(Li) + Li]^+$	1,424	1,452	1,748	1,776
Products of $[M(Li) + Li]^+$				
B. $[Y_n(Li) + Li]^+$ and ceramide-related				
$[M(Li) - Hex + Li]^+$	1,262	1,290	1,586	1,614
$[M(Li) - 2Hex + Li]^+$	1,100	1,128	1,424	1,452
$[M(Li) - 3Hex + Li]^+$	938	966	1,262	1,290
$[M(Li) - 4Hex + Li]^+$	—	—	1,100	1,128
$[M(Li) - 5Hex + Li]^+$	—	—	938	966
$[Y_0PO_3(Li) + Li]^+$	776	804	776	804
$[Z_0PO_3(Li) + Li]^+$	758	786	758	786
$[Z_0PO_3(Li) + Li - H_2O]^+$	740V[a]	768	740V[a]	768
$[Y_0 + Li]^+$	690	718	690	718
$[Z_0 + Li]^+$	672V[a]	700	672V[a]	700
$[O/Z_0PO_3(Li) + Li]^+$	392	420	392	420
C. Loss of part or all of acyl chain				
$[J(Li) + Li]^+$	1,086	1,114	1,410	1,438
$[J(Li) + Li - H_2O)]^+$	1,068	1,096	1,392	1,420
$[O(Li) + Li]^+$	1,058	1,086	1,382	1,410
Products of $[Y_0 + Li]^+$				
D. Sphingoid-related				
$[J/Y_0 + Li - H_2O]^+$	334	362	334	362
$[N + Li]^+ \equiv [O/Y_0 + Li]^+$	324	352	324	352
$[N + Li - H_2O]^+$	306	334	306	334
$[N + Li - 2H_2O]^+$	288	316	288	316
$[N + Li - H_2O - CH_2O]^+$	276	304	276	304
d_{3b}	291	319	291	319
c_{1b}[b]	263	291	263	291
E. Fatty-*N*-acyl-related				
$[S + Li]^+ \equiv [G/Y_0 + Li - H_2]^+$	432	432	432	432
$[T + Li]^+ \equiv [G/Z_0 + Li]^+$	416	416	416	416
$[U + Li]^+ \equiv [T + Li - C_2H_2]^+$	390	390	390	390
$[U + Li - H_2O]^+$	372	372	372	372
$[W + Li]^+ \equiv [\text{acyl } C_2 - C_\omega + Li]^+$	345	345	345	345

Fragment designations as in Costello and Vath (75), as expanded for GIPCs in Singh, Costello, and Beach (74), with modifications of Adams and Ann (73) for ceramide-derived ions; illustrated in Schemes 2–4. Additional designations ($\underline{d}_{3b}$ and $\underline{c}_{1b}$) from Hsu and Turk (57) for ceramide-derived ions (structures shown in Scheme 2C,E).

[a] V = overlapped with major glycosylinositol ions.

[b] Incorrectly designated $\underline{d}_{3b}-H_2O$ in (46).

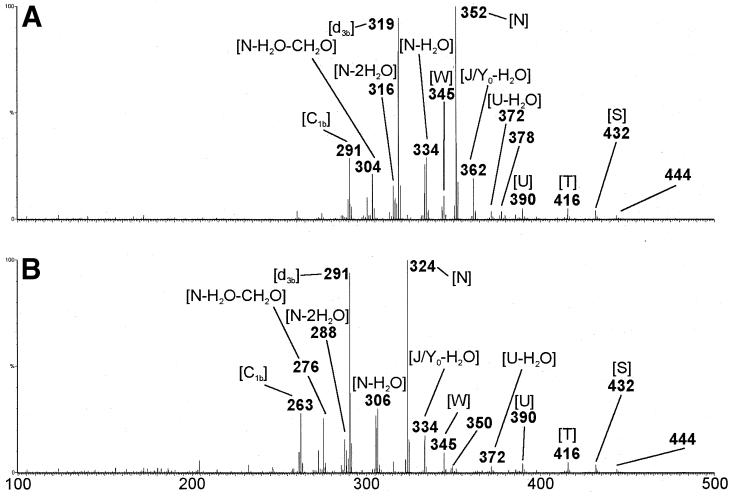

Fig. 6. High extraction cone voltage $^{+}$ESI-Qq/oa-TOF spectra of An-3. Expansions (m/z 200–500) of tandem ESI-CID-MS/CID-MS product ion spectra from $[Y_0 + Li]^+$ of An-3. A: Products of $[Y_0 + Li]^+$ at m/z 718. B: Products of $[Y_0 + Li]^+$ at m/z 690. The adduct designation "+Li" and the charge form have been omitted from the fragment labels for clarity.

point}, consistent with pentahexosylinositolphosphate as a dilithiated salt adduct. As shown in detail for the m/z 1,748 adduct (Fig. 7C, D), complete series of glycosidic cleavage ions {$[Y_m/C_nPO_3(Li) + Li]^+$, $[Y_m/B_nPO_3(Li) + Li]^+$, $[C_n + Li]^+$, $[B_n + Li]^+$, $[Y_m/C_n + Li]^+$, and $[Y_m/B_n + Li]^+$} were observed, along with $[Z_m/B_nPO_3(Li) + Li]^+$ and $[Z_m/B_n + Li]^+$ ions (see Table 3). Similar to the observation with An-3, a much lower abundance was observed for fragment ions at m/z 417 and 435, compared with other ions in the glycosylinositol phosphate series. In particular, the ratios of the relative abundances of m/z 435 versus m/z 273 (0.27), and m/z 435 versus m/z 597 (0.17), were consistent with the presence of a single branch point in the glycan at the same monosaccharide residue as An-3 (see **Scheme 4**, where m/z 417 and 435 represent ions requiring at least two glycosidic cleavages for their appearance, $[Y_{2\alpha}/Y_{2\beta}/B_5PO_3(Li) + Li]^+$ and $[Y_{2\alpha}/Y_{2\beta}/C_5PO_3(Li) + Li]^+$, respectively). The location of this branch point is consistent with extension of one of the nonreducing terminal Man residues of An-3 with two additional residues in a continuous chain. Different branching structures (e.g., symmetric extension of each of the nonreducing terminal Man residues of An-3 with one additional residue, or the presence of a second branch point in the structure), are contraindicated by the observation of all remaining $[Y_m/C_nPO_3(Li) + Li]^+$ and $[Y_m/B_nPO_3(Li) + Li]^+$ series ions in high abundance.

As observed with An-3, $[Y_m(Li) + Li]^+$, fragments de-

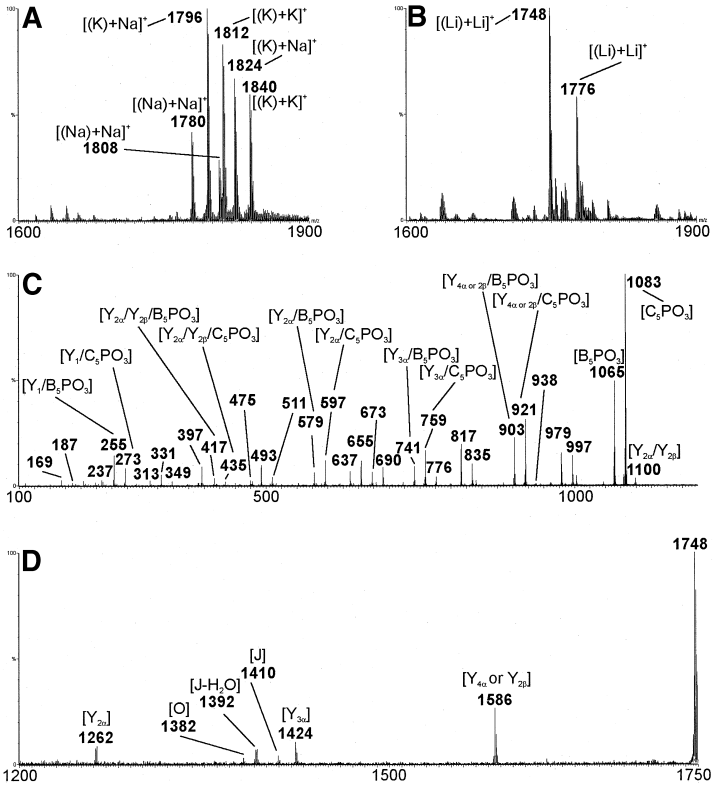

Fig. 7. $^{+}$ESI-Qq/oa-TOF spectra of An-5. A: Profile of molecular ions as mixed $[M(Na) + Na]^+$, $[M(K) + K]^+$, and $[M(Na) + K]^+$ {or $[M(K) + Na]^+$} adducts. B: Simplified profile of molecular ions as $[M(Li) + Li]^+$ adducts. C: MS/CID-MS of $[M(Li) + Li]^+$ at m/z 1,748, low m/z region. D: MS/CID-MS of $[M(Li) + Li]^+$ at m/z 1,748, high m/z region. The Y-axis expansion in D relative to C is 9×. Ion designations correspond to Scheme 4. The designations "+Li" and "(Li) + Li" and the charge form have been omitted from the fragment labels for clarity.

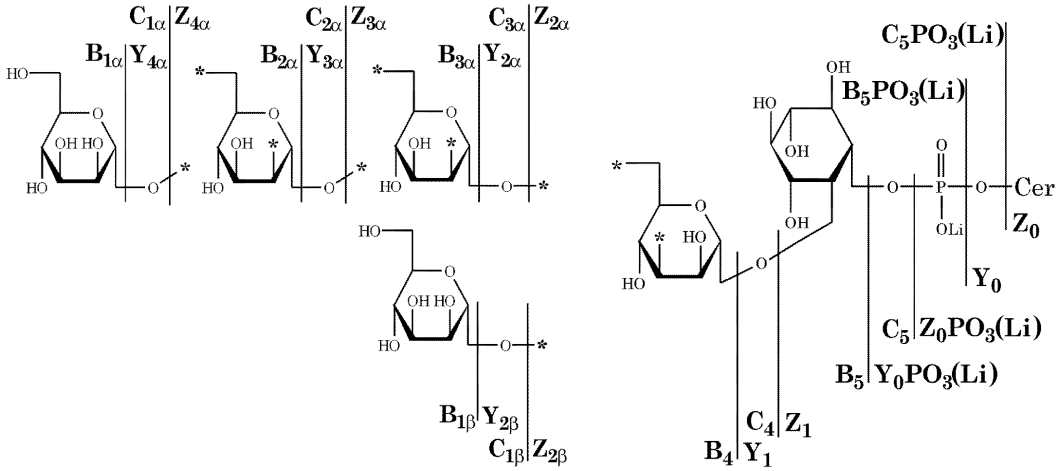

Scheme 4. Fragmentation of GIPC An-5 in positive-ion ESI-Qq/oa-TOF-MS; ion designations according to Costello and Vath (75), and Singh, Costello, and Beach (74). The adduct designation "+Li" and the charge form have been omitted from the labels for clarity.

rived from sequential loss of monosaccharide residues from $[M(Li) + Li]^+$ appeared at low abundance in the $^+$ESI-Q/q(CID)-oa-TOF-MS of An-5 (Fig. 7C, D, Table 4). Ceramide and ceramide phosphate ions {$[Y_0 + Li]^+$, $[Z_0 + Li]^+$, $[Y_0PO_3(Li) + Li]^+$, and $[Z_0PO_3(Li) + Li]^+$} appeared as well in the product ion spectra of An-5 at intermediate abundances. As with An-3, ions lacking all or part of the acyl chain {$[O(Li) + Li]^+$, $[J(Li) + Li]^+$, and $[J(Li) + Li - H_2O)]^+$} indicated that the *m/z* 28 increment between the two predominant molecular species is primarily due to a corresponding C_2H_4 difference in the sphingoid rather than the *N*-acyl chain. This was again confirmed by product ion spectra generated via $^+$ESI-(CID)-Q/q(CID)-oa-TOF-MS from the primary $[Y_0 + Li]^+$ ions at *m/z* 690 and 718 observed in the high extraction cone voltage profile of An-5. These pseudo-$^+$ESI-(CID-MS)^2 spectra (not shown) were essentially identical to those acquired from the same ions of An-3. Thus, major $[N + Li]^+$ and $\underline{d}_{3b}$ fragments are again observed at *m/z* 324 and 291 in the spectrum of products from *m/z* 690, and at *m/z* 352 and 319 in the spectrum from *m/z* 718. All of these results are summarized in Tables 3 and 4.

Quantitation of *A. nidulans* GIPCs

Having established that the major orcinol-positive bands, visible in HPTLC of the crude base-stable acidic lipids (Fig. 1A, lane C), are GIPCs incorporating an increasing number of Man residues, we made a crude estimate of their molar proportions by densitometric analysis of these bands, whose staining could now be "normalized" by the relative hexose content of each component (for this purpose, An-4 was assumed to be a tetrahexosyl IPC). This analysis yielded approximate molar proportions of 1:5:0.1:0.4 (estimated error ±20%) for An-2, An-3, An-4, and An-5, respectively. Note that the usefulness of these values should be judged against our observations that the overall yield and proportion of GIPCs from *A. nidulans* and other fungi can vary between strains and depend considerably as well on culture medium, temperature, and stage of growth. On the basis of these caveats, as well as the fact that extractions were performed on fresh, wet mycelium, no attempt was made to calculate the yield of GIPCs relative to cellular mass for this study, as such values could not be considered reproducible.

DISCUSSION

Recent investigations of GSL biosynthesis and function in fungi have focused on *Aspergillus nidulans*, a nonpathogenic laboratory model for the opportunistic mycopathogen, *A. fumigatus*. As has been observed with many other fungi, GSL biosynthesis in *A. nidulans* is partitioned into two major pathways, one for production of GIPCs, and another leading to accumulation of cerebrosides [β-galactosylceramide (GalCer) and/or β-glucosylceramide (GlcCer)]. In a previous study (36), we characterized a GlcCer from *A. nidulans* and observed that strong inhibitors of GlcCer synthase interfered with germination, cell cycle, and hyphal growth in both *A. nidulans* and *A. fumigatus*, suggesting that GlcCer biosynthesis is essential in these fungi and that design of inhibitors more specific for the fungal enzyme than for the mammalian one might offer a potential route to a new class of antifungal agents. On the other hand, it is already well appreciated that disruption of the GIPC pathway, by either inhibition or deletion of IPC synthase activity, is fatal for fungi (24–27, 29, 30), except for some yeast strains with compensating mutations (58–60). Some fungal strains selected for resistance to the IPC synthase inhibitor Aureobasidin A were found to have a mutation in the *AUR1* gene that affects the interaction of the AUR1 protein with the drug but not catalytic activity (25–27, 29). Overexpression of the *AUR1* gene in *S. pombe* conferred significant resistance to Aureobasidin A (25); in addition, wild-type strains of some fungal species, such as the mycopathogen *A. fumigatus*, are relatively resistant by virtue of highly efficient transporter-mediated drug efflux (61). Exploitation of IPC synthase inhibitors as antifungal

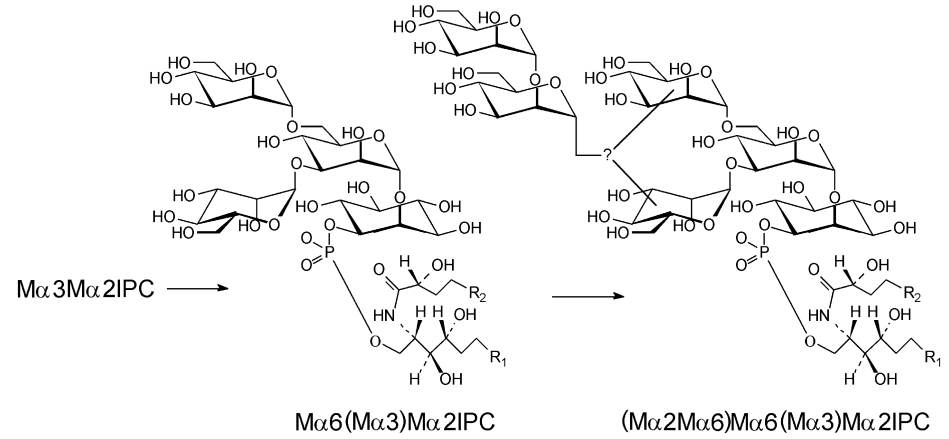

Scheme 5. Structures and hypothetical biosynthetic relationships of complex *A. nidulans* GIPCs starting with Mα3Mα2IPC. Linkage positions marked by (?) are as yet undetermined.

drugs is already being investigated, but generation of new therapeutic candidates will doubtless have to address issues of fungal resistance (33).

Recent detailed studies have demonstrated that GIPC biosynthesis is essential for normal cell cycle progression and polarized growth in *A. nidulans* (35). To dissect further the possible functional role(s) of fungal GIPC biosynthesis, and perhaps exploit glycosyltransferases specific to this pathway for the development of other antifungal agents, we have sought to characterize GIPC expression in *Aspergillus* species in more detail, beginning with studies to establish the structures of GIPCs in the model fungus *A. nidulans*. From the current study, the GIPC profile of *A. nidulans* appears to be relatively simple, with expression of only three significant components, all bearing oligo-α-mannose-type glycans. These are:

$$\text{Man}\alpha1\rightarrow3\text{Man}\alpha1\rightarrow2\text{Ins-P-Cer} \quad \text{An-2}$$

$$\begin{matrix}\text{Man}\alpha1\rightarrow6\\ \qquad\qquad\text{Man}\alpha1\rightarrow2\text{Ins-P-Cer}\\ \text{Man}\alpha1\rightarrow3\end{matrix} \quad \text{An-3}$$

$$\text{Man}\alpha1\rightarrow2?\text{Man}\alpha1\rightarrow6?\begin{cases}\text{Man}\alpha1\rightarrow6\\ \qquad\qquad\text{Man}\alpha1\rightarrow2\text{Ins-P-Cer}\\ \text{Man}\alpha1\rightarrow3\end{cases} \quad \text{An-5}$$

The presence of some minor components could be detected, but sufficient material was not obtained for their analysis. The possibility exists that these minor components could possess very different glycans, perhaps bearing sugar residues other than mannose; moreover, other components could be expressed by *A. nidulans*, perhaps under different conditions or by different strains. However, a similar profile, showing essentially three major (along with some minor) GIPC bands, was also obtained from a different wild-type *A. nidulans* strain (A773), although no detailed structural characterization was reported in that work (35). The structures proposed herein for the three major *A. nidulans* GIPC components suggest a single biosynthetic pathway connecting them, as depicted in **Scheme 5**.

In general, knowledge about structures of fungal GIPCs is still at an early stage, with only a handful of species having been examined so far. The present study is the first to report detailed characterization of GIPCs from an *Aspergillus* species. Among the Aspergilli, early attempts at characterization of GIPC structure and biosynthesis were initiated with *A. niger* (62–64); compositional analysis indicated that the structures were complex, but characterizations beyond this point were not published. The first detailed characterizations of complex GIPCs (containing more than one monosaccharide residue) from a Euascomycete fungal species were carried out in the 1980s by Robert Lester and his colleagues (16, 65). In these key early studies, the major GIPCs from both the yeast and mycelial forms of the dimorphic mycopathogen *Histoplasma capsulatum* were profiled, isolated, and analyzed by MS, GC-MS, and degradative methods. The primary structures of three GIPCs were established completely except for the precise linkage of the first sugar residue to the *myo*-inositol ring, which was proposed to be either Manα1→2Ins or Manα1→6Ins.[1] A decade and a half later, the first unambiguous determination of this core linkage was published for GIPCs of a related dimorphic mycopathogen, *Paracoccidioides brasiliensis*, where it was shown to be Manα1→2Ins (45). Subsequent studies have shown this to be an important detail, because GIPC series with both Manα1→2Ins or Manα1→6Ins core linkages are now known (54, 66). More recently, a major component of the yeast form of a third dimorphic mycopathogen, *S. schenckii*, was found to possess an additional core linkage, $GlcNH_2\alpha1\rightarrow2$Ins (53), so that three distinct monosaccharide linkages to *myo*-Ins have now been identified for GIPCs of Ascomycete fungal species. In the present study, only one core structure, Manα1→2Ins, was observed for the GIPCs of *A. nidulans*.

[1] Although Barr, Laine, and Lester (65) did not specify precisely the linkage between Man and Ins in their compounds, but characterized it as Manα1→2/6Ins, NMR spectroscopy of *H. capsulatum* GIPCs shows that the linkage is Manα1→2Ins1-P-1Cer (S. B. Levery, M. S. Toledo, A. H. Straus, and H. K. Takahashi, unpublished observations), as reported for GIPCs of the closely related fungus, *P. brasiliensis* (45).

Biosynthesis of the M_3IPC (An-3) from IPC presumably requires the action of at least three distinct α-mannosyltransferase activities. In *S. cerevisiae*, two genes, *SUR1* (*CSG1/BCL21*) and *CSG2* (*CLS2*), are apparently required for production of MIPC (most likely Manα2IPC) (67, 68). Of these, the latter does not resemble a glycosyltransferase ("glycosyl-T") gene (67, 69), and its product has not been found in the Golgi but in the endoplasmic reticulum (70); the CSG2 protein is thought to be an integral membrane protein with a role in regulation of Ca^{2+} levels in the endoplasmic reticulum (67, 69), although its true function has not been verified. The SUR1 protein, on the other hand, does incorporate a domain with substantial identity to a known α1,6-Man-T (Och1p) (68), and is therefore considered a likely candidate for a true MIPC synthase. Nothing is known about the presumed α1,3-Man-T responsible for synthesis of the common intermediate M_2IPC (An-2) or about glycosyltransferases involved in any of the subsequent steps in synthesis of more complex GIPCs (such as the α1,6-Man-T required to convert An-2 to An-3 in *A. nidulans*).

As a number of confirmed or putative genes for α1,2-, α1,3-, and α1,6-Man-Ts are known, an interesting point to determine is whether the downstream glycosylation steps in the biosynthesis of oligo-α-mannosyl IPCs such as An-3 are carried out by α-man-Ts also used in other pathways, or by enzymes specific to the GIPC pathway, and therefore among candidates with as yet unconfirmed glycosyltransferase functions. Examples of both overlapping and nonoverlapping pathway specificities are known from studies of mammalian glycosyltransferase families such as the Galβ1,3- and Galβ1,4-Ts (71). Another key question is whether biosynthesis of MIPC or more highly elaborated GIPCs is essential for the survival of fungi. It has been established that biosynthesis of IPC is required for vegetative growth of *S. cerevisiae* (24) but that conversion to MIPC is not (68); however, this finding doesn't exclude essential roles for MIPC, M_2IPC, and further GIPC products in *A. nidulans* or other higher fungi. If they have essential roles, then glycosyltransferases downstream of IPC synthase could be targets of inhibitors with potential as antifungal agents, provided they are specific to GIPC biosynthesis.

The identity of the glycosylinositol structure of the *A. nidulans* M_3IPC with that of *C. cibarius* is somewhat surprising, insofar as these fungi are members of evolutionarily distant phyla (Ascomycota and Basidiomycota, respectively). However, the *C. cibarius* GIPC profile also appears to be distinct from those of all seven other Basidiomycete species examined so far, in that the core structures of the latter all diverge at the point of adding the second monosaccharide residue (Galβ1→6Manα1→2Ins) (55, 72). In any case, GIPCs more polar than M_3IPC were not observed in the *C. cibarius* profile, as found here for *A. nidulans*. A more critical comparison awaits characterization of the GIPCs of *A. fumigatus*. Preliminary evidence indicates a number of differences between the GIPCs of *A. fumigatus* and those found in *A. nidulans* (M. S. Toledo, B. Bennion, C. Park, S. B. Levery, A. H. Straus, and H. K. Takahashi, unpublished observations). The current work suggests that genomic and/or proteomic comparisons should help to identify candidate glycosyltransferases (or other factors controlling GIPC expression) that are present in *A. fumigatus* and absent in *A. nidulans*. Because many genes in the two species are mutually complementary (37–41), *A. nidulans* would be an excellent vehicle for testing the effects of transformation by genes putatively responsible for the distinct profile of GIPCs expressed in *A. fumigatus*.

This work was supported by the New Hampshire Biological Research Infrastructure Network-Center for Structural Biology (NIH Grant P20 RR-16459), the National Institutes of Health Resource Center for Biomedical Complex Carbohydrates (NIH Grant P41 RR-05351), National Institutes of Health Grant R01 GM-54045, and a Glycoscience Research Award from Neose Technologies, Inc. (S.B.L); and by DOE Biosciences grant DE-FG02-97ER20275 and a Burroughs Wellcome New Investigator Award in Pathogenic Mycology (M.M.). The authors wish to thank Emma Arigi for technical assistance with the GC-MS analysis.

REFERENCES

1. Lortholary, O., D. W. Denning, and B. Dupont. 1999. Endemic mycoses: a treatment update. *J. Antimicrob. Chemother.* **43:** 321–331.
2. Wade, J. C. 1997. Treatment of fungal and other opportunistic infections in immunocompromised patients. *Leukemia.* **11 (Suppl. 4):** 38–39.
3. Walsh, T. J., J. W. Hiemenz, and E. Anaissie. 1996. Recent progress and current problems in treatment of invasive fungal infections in neutropenic patients. *Infect. Dis. Clin. North Am.* **10:** 365–400.
4. van Burik, J. A., and P. T. Magee. 2001. Aspects of fungal pathogenesis in humans. *Annu. Rev. Microbiol.* **55:** 743–772.
5. Latge, J. P., and R. Calderone. 2002. Host-microbe interactions: fungi invasive human fungal opportunistic infections. *Curr. Opin. Microbiol.* **5:** 355–358.
6. Moore, C. B., N. Sayers, J. Mosquera, J. Slaven, and D. W. Denning. 2000. Antifungal drug resistance in Aspergillus. *J. Infect.* **41:** 203–220.
7. Cowen, L. E., J. B. Anderson, and L. M. Kohn. 2002. Evolution of drug resistance in Candida albicans. *Annu. Rev. Microbiol.* **56:** 139–165.
8. Kontoyiannis, D. P., and R. E. Lewis. 2002. Antifungal drug resistance of pathogenic fungi. *Lancet.* **359:** 1135–1144.
9. Sanglard, D. 2002. Resistance of human fungal pathogens to antifungal drugs. *Curr. Opin. Microbiol.* **5:** 379–385.
10. Viscoli, C., and E. Castagnola. 1998. Emerging fungal pathogens, drug resistance and the role of lipid formulations of amphotericin B in the treatment of fungal infections in cancer patients: a review. *Int. J. Infect. Dis.* **3:** 109–118.
11. Walsh, T. J., and A. H. Groll. 1999. Emerging fungal pathogens: evolving challenges to immunocompromised patients for the twenty-first century. *Transpl. Infect. Dis.* **1:** 247–261.
12. Ponton, J., R. Ruchel, K. V. Clemons, D. C. Coleman, R. Grillot, J. Guarro, D. Aldebert, P. Ambroise-Thomas, J. Cano, A. J. Carrillo-Munoz, J. Gene, C. Pinel, D. A. Stevens, and D. J. Sullivan. 2000. Emerging pathogens. *Med. Mycol.* **38 (Suppl. 1):** 225–236.
13. Dickson, R. C., and R. L. Lester. 1999. Yeast sphingolipids. *Biochim. Biophys. Acta.* **1426:** 347–357.
14. Dickson, R. C., and R. L. Lester. 1999. Metabolism and selected functions of sphingolipids in the yeast *Saccharomyces cerevisiae*. *Biochim. Biophys. Acta.* **1438:** 305–321.
15. Dickson, R. C., and R. L. Lester. 2002. Sphingolipid functions in *Saccharomyces cerevisiae*. *Biochim. Biophys. Acta.* **1583:** 13–25.
16. Barr, K., and R. L. Lester. 1984. Occurrence of novel antigenic phosphoinositol-containing sphingolipids in the pathogenic yeast *Histoplasma capsulatum*. *Biochemistry.* **23:** 5581–5588.
17. Suzuki, E., M. S. Toledo, H. K. Takahashi, and A. H. Straus. 1997. A

monoclonal antibody directed to terminal residue of β-galactofuranose of a glycolipid antigen isolated from *Paracoccidioides brasiliensis*: cross-reactivity with *Leishmania major* and *Trypanosoma cruzi*. *Glycobiology.* **7:** 463–468.
18. Straus, A. H., E. Suzuki, M. S. Toledo, C. M. Takizawa, and H. K. Takahashi. 1995. Immunochemical characterization of carbohydrate antigens from fungi, protozoa and mammals by monoclonal antibodies directed to glycan epitopes. *Braz. J. Med. Biol. Res.* **28:** 919–923.
19. Toledo, M. S., E. Suzuki, A. H. Straus, and H. K. Takahashi. 1995. Glycolipids from *Paracoccidioides brasiliensis*. Isolation of a galactofuranose-containing glycolipid reactive with sera of patients with paracoccidioidomycosis. *J. Med. Vet. Mycol.* **33:** 247–251.
20. Jennemann, R., B. L. Bauer, H. Bertalanffy, T. Selmer, and H. Wiegandt. 1999. Basidiolipids from *Agaricus* are novel immune adjuvants. *Immunobiology.* **200:** 277–289.
21. Jennemann, R., R. Sandhoff, H-J. Grone, and H. Wiegandt. 2001. Human heterophile antibodies recognizing distinct carbohydrate epitopes on basidiolipids from different mushrooms. *Immunol. Invest.* **30:** 115–129.
22. Funato, K., B. Vallee, and H. Riezman. 2002. Biosynthesis and trafficking of sphingolipids in the yeast Saccharomyces cerevisiae. *Biochemistry.* **41:** 15105–15114.
23. Wells, G. B., and R. L. Lester. 1983. The isolation and characterization of a mutant strain of *Saccharomyces cerevisiae* that requires a long chain base for growth and for synthesis of phosphosphingolipids. *J. Biol. Chem.* **258:** 10200–10203.
24. Nagiec, M. M., E. E. Nagiec, J. A. Baltisberger, G. B. Wells, R. L. Lester, and R. C. Dickson. 1997. Sphingolipid synthesis as a target for antifungal drugs. Complementation of the inositol phosphorylceramide synthase defect in a mutant strain of *Saccharomyces cerevisiae* by the *AUR1* gene. *J. Biol. Chem.* **272:** 9809–9817.
25. Hashida-Okado, T., R. Yasumoto, M. Endo, K. Takesako, and I. Kato. 1998. Isolation and characterization of the aureobasidin A-resistant gene, aur1R, on *Schizosaccharomyces pombe*: roles of Aur1p + in cell morphogenesis. *Curr. Genet.* **33:** 38–45.
26. Kuroda, M., T. Hashida-Okado, R. Yasumoto, K. Gomi, I. Kato, and K. Takesako. 1999. An aureobasidin A resistance gene isolated from Aspergillus is a homolog of yeast AUR1, a gene responsible for inositol phosphorylceramide (IPC) synthase activity. *Mol. Gen. Genet.* **261:** 290–296.
27. Heidler, S. A., and J. A. Radding. 1995. The *AUR1* gene in *Saccharomyces cerevisiae* encodes a dominant resistance to the antifungal agent Aureobasidin A (LY295337). *Antimicrob. Agents Chemother.* **39:** 2765–2769.
28. Heidler, S. A., and J. A. Radding. 2000. Inositol phosphoryl transferases from human pathogenic fungi. *Biochim. Biophys. Acta.* **1500:** 147–152.
29. Hashida-Okado, T., A. Ogawa, M. Endo, R. Yasumoto, K. Takesako, and I. Kato. 1996. *AUR1*, a novel gene conferring aureobasidin resistance on *Saccharomyces cerevisiae*: a study of defective morphologies in Aur1p-depleted cells. *Mol. Gen. Genet.* **251:** 236–244.
30. Takesako, K., H. Kuroda, T. Inoue, F. Haruna, Y. Yoshikawa, and I. Kato. 1993. Biological properties of Aureobasidin A, a cyclic depsipeptide antifungal antibiotic. *J.Antibiot.* **49:** 1414–1420.
31. Mandala, S. M., R. A. Thornton, M. Rosenbach, J. Milligan, M. Garcia-Calvo, H. G. Bull, and M. B. Kurtz. 1997. Khafrefungin, a novel inhibitor of sphingolipid synthesis. *J. Biol. Chem.* **272:** 32709–32714.
32. Mandala, S. M., R. A. Thornton, J. Milligan, M. Rosenbach, M. Garcia-Calvo, H. G. Bull, G. Harris, G. K. Abruzzo, A. M. Flattery, C. J. Gill, S. Bartizal, and M. B. Kurtz. 1998. Rustmicin, a potent antifungal agent, inhibits sphingolipid synthesis at the inositol phosphoceramide synthase. *J. Biol. Chem.* **273:** 14942–14949.
33. Georgopapadakou, N. H. 2000. Antifungals targeted to sphingolipid synthesis: focus on inositol phosphorylceramide synthase. *Expert Opin. Investig. Drugs.* **9:** 1787–1796.
34. Luberto, C., D. L. Toffaletti, E. A. Wills, S. C. Tucker, A. Casadevall, J. R. Perfect, Y. A. Hannun, and M. Del Poeta. 2001. Roles for inositol-phosphoryl ceramide synthase (*IPC1*) in pathogenesis of *C. neoformans*. *Genes Dev.* **15:** 201–212.
35. Cheng, J., T-S. Park, A. S. Fischl, and X. S. Ye. 2001. Cell cycle progression and cell polarity require sphingolipid biosynthesis in *Aspergillus nidulans*. *Mol. Cell. Biol.* **21:** 6198–6209.
36. Levery, S. B., M. Momany, R. Lindsey, M. S. Toledo, J. A. Shayman, M. Fuller, K. Brooks, R. L. Doong, A. H. Straus, and H. K. Takahashi. 2002. Disruption of the glucosylceramide biosynthesis pathway in *Aspergillus nidulans* and *Aspergillus fumigatus* by inhibitors of UDP-Glc: ceramide glucosyltransferase strongly affects spore germination, cell cycle, and hyphal growth. *FEBS Lett.* **525:** 59–64.
37. Borgia, P. T., C. L. Dodge, L. E. Eagleton, and T. H. Adams. 1994. Bidirectional gene transfer between *Aspergillus fumigatus* and *Aspergillus nidulans*. *FEMS Microbiol. Lett.* **122:** 227–231.
38. Horiuchi, H., and M. Takagi. 1999. Chitin synthase genes of *Aspergillus* species. *Contrib. Microbiol.* **2:** 193–204.
39. Momany, M., and I. Taylor. 2000. Landmarks in the early duplication cycles of *Aspergillus fumigatus* and *Aspergillus nidulans*: polarity, germ tube emergence and septation. *Microbiol.* **146:** 3279–3284.
40. Brakhage, A. A., and K. Langfelder. 2002. Menacing mold: the molecular biology of Aspergillus fumigatus. *Annu. Rev. Microbiol.* **56:** 433–455.
41. Latge, J. P. 2001. The pathobiology of *Aspergillus fumigatus*. *Trends Microbiol.* **9:** 382–389.
42. Kafer, E. 1977. Meiotic and mitotic recombinations in *Aspergillus* and its chromosomal aberrations. *Adv. Genet.* **19:** 33–131.
43. Toledo, M. S., S. B. Levery, A. H. Straus, E. Suzuki, M. Momany, J. Glushka, J. M. Moulton, and H. K. Takahashi. 1999. Characterization of sphingolipids from mycopathogens: factors correlating with expression of 2-hydroxy fatty acyl (*E*)-Δ^3-unsaturation in cerebrosides of *Paracoccidioides brasiliensis* and *Aspergillus fumigatus*. *Biochemistry.* **38:** 7294–7306.
44. Dabrowski, J., P. Hanfland, and H. Egge. 1980. Structural analysis of glycosphingolipids by high-resolution ^{1}H nuclear magnetic resonance spectroscopy. *Biochemistry.* **19:** 5652–5658.
45. Levery, S. B., M. S. Toledo, A. H. Straus, and H. K. Takahashi. 1998. Structure elucidation of sphingolipids from the mycopathogen *Paracoccidioides brasiliensis*: an immunodominant β-galactofuranose residue is carried by a novel glycosylinositol phosphorylceramide antigen. *Biochemistry.* **37:** 8764–8775.
46. Levery, S. B., M. S. Toledo, A. H. Straus, and H. K. Takahashi. 2001. Comparative analysis of glycosylinositol phosphorylceramides from fungi by electrospray tandem mass spectrometry with low-energy collision-induced dissociation of Li^+ adduct ions. *Rapid Commun. Mass Spectrom.* **15:** 2240–2258.
47. Laine, R. A., N. D. Young, J. N. Gerber, and C. C. Sweeley. 1974. Identification of 2-hydroxy fatty acids in complex mixtures of fatty acid methyl esters by mass chromatography. *Biomed. Mass Spectrom.* **1:** 10–14.
48. Thorpe, S. R., and C. C. Sweeley. 1967. Chemistry and metabolism of sphingolipids. On the biosynthesis of phytosphingosine by yeast. *Biochemistry.* **6:** 887–897.
49. Gaver, R. C., and C. C. Sweeley. 1966. Chemistry and metabolism of sphingolipids. 3-Oxo derivatives of *N*-acetylsphingosine and *N*-acetyldihydrosphingosine. *Biochemistry.* **88:** 3643–3647.
50. Polito, A. J., T. Akita, and C. C. Sweeley. 1968. Gas chromatography and mass spectrometry of sphingolipid bases. Characterization of sphinga-4,14-dienine from plasma sphingomyelin. *Biochemistry.* **7:** 2609–2614.
51. Vliegenthart, J. F. G., L. Dorland, and H. van Halbeek. 1983. High-resolution ^{1}H-nuclear magnetic resonance spectroscopy as a tool in the structural analysis of carbohydrates related to glycoproteins. *Adv. Carbohydr. Chem. Biochem.* **41:** 209–374.
52. Fu, D., L. Chen, and R. A. O'Neill. 1994. A detailed structural characterization of ribonuclease B oligosaccharides by ^{1}H-NMR spectroscopy and mass spectrometry. *Carbohydr. Res.* **261:** 173–186.
53. Toledo, M. S., S. B. Levery, A. H. Straus, and H. K. Takahashi. 2001. Sphingolipids of the mycopathogen *Sporothrix schenckii*: identification of a glycosylinositol phosphorylceramide with novel core $GlcNH_2\alpha1\rightarrow2Ins$ motif. *FEBS Lett.* **493:** 50–56.
54. Toledo, M. S., S. B. Levery, J. Glushka, A. H. Straus, and H. K. Takahashi. 2001. Structure elucidation of sphingolipids from the mycopathogen *Sporothrix schenckii*: identification of novel glycosylinositol phosphorylceramides with core $Man\alpha1\rightarrow6Ins$ linkage. *Biochem. Biophys. Res. Commun.* **280:** 19–24.
55. Jennemann, R., R. Geyer, R. Sandhoff, R. M. Gschwind, S. B. Levery, H-J. Gröne, and H. Wiegandt. 2001. Glycoinositolphosphosphingolipids (basidiolipids) of higher mushrooms. *Eur. J. Biochem.* **268:** 1190–1205.
56. Gorin, P. A. J. 1981. Carbon-13 nuclear magnetic resonance spectroscopy of polysaccharides. *Adv. Carbohydr. Chem. Biochem.* **38:** 13–104.
57. Hsu, F-F., and J. Turk. 2001. Structural determination of glycosphingolipids as lithiated adducts by electrospray ionization mass spectrometry using low-energy collisional-activated dissociation on a

triple stage quadrupole instrument. *J. Am. Soc. Mass Spectrom.* **12:** 61–79.
58. Dickson, R. C., G. B. Wells, A. Schmidt, and R. L. Lester. 1990. Isolation of mutant S*accharomyces cerevisiae* strains that survive without sphingolipid. *Mol. Cell. Biol.* **10:** 2176–2181.
59. Nagiec, M. M., G. B. Wells, R. L. Lester, and R. C. Dickson. 1993. A suppressor gene that enables *Saccharomyces cerevisiae* to grow without making sphingolipids encodes a protein that resembles an *Escherichia coli* fatty acyltransferase. *J. Biol. Chem.* **268:** 22156–22163.
60. Lester, R. L., G. B. Wells, G. Oxford, and R. C. Dickson. 1993. Mutant strains of *Saccharomyces cerevisiae* lacking sphingolipids synthesize novel inositol glycerophospholipids that mimic sphingolipid structures. *J. Biol. Chem.* **268:** 845–856.
61. Zhong, W., M. W. Jeffries, and N. H. Georgopapadakou. 2000. Inhibition of inositol phosphorylceramide synthase by aureobasidin A in Candida and Aspergillus species. *Antimicrob. Agents Chemother.* **44:** 651–653.
62. Brennan, P. J., and J. Roe. 1975. The occurrence of a phosphorylated glycosphingolipid in *Aspergillus niger. Biochem. J.* **147:** 179–180.
63. Byrne, P. F., and P. J. Brennan. 1976. Isolation and characterization of inositol-containing glycosphingolipids from *Aspergillus niger. Biochem. Soc. Trans.* **4:** 893–895.
64. Hackett, J. A., and P. J. Brennan. 1977. The isolation and biosynthesis of the ceramide-phosphoinositol of *Aspergillus niger. FEBS Lett.* **74:** 259–263.
65. Barr, K., R. A. Laine, and R. L. Lester. 1984. Carbohydrate structures of three novel phosphoinositol-containing sphingolipids from the yeast *Histoplasma capsulatum. Biochemistry.* **23:** 5589–5596.
66. Loureiro y Penha, C. V., A. R. Todeschini, L. M. Lopes-Bezerra, R. Wait, C. Jones, K. A. Mattos, N. Heise, L. Mendonca-Previato, and J. O. Previato. 2001. Characterization of novel structures of mannosylinositolphosphorylceramides from the yeast forms of *Sporothrix schenckii. Eur. J. Biochem.* **268:** 4243–4250.
67. Zhao, C., T. Beeler, and T. Dunn. 1994. Suppressors of the Ca^{2+}-sensitive yeast mutant (*csg2*) identify genes involved in sphingolipid biosynthesis. Cloning and characterization of *SCS1*, a gene required for serine palmitoyltransferase activity. *J. Biol. Chem.* **269:** 21480–21488.
68. Beeler, T. J., D. Fu, J. Rivera, E. Monaghan, K. Gable, and T. M. Dunn. 1997. *SUR1* (*CSG1/BCL21*), a gene necessary for growth of *Saccharomyces cerevisiae* in the presence of high Ca^{2+} concentrations at 37° C, is required for mannosylation of inositolphosphorylceramide. *Mol. Gen. Genet.* **255:** 570–579.
69. Beeler, T., K. Gable, C. Zhao, and T. Dunn. 1994. A novel protein, CSG2p, is required for Ca^{2+} regulation in *Saccharomyces cerevisiae. J. Biol. Chem.* **269:** 7279–7284.
70. Tanida, I., Y. Takita, A. Hasegawa, Y. Ohya, and Y. Anraku. 1996. Yeast Cls2p/Csg2p localized on the endoplasmic reticulum membrane regulates a non-exchangeable intracellular Ca2+ pool cooperatively with calcineurin. *FEBS Lett.* **379:** 38–42.
71. Amado, M., R. Almeida, T. Schwientek, and H. Clausen. 1999. Identification and characterization of large galactosyltransferase gene families: galactosyltransferases for all functions. *Biochim. Biophys. Acta.* **1473:** 35–53.
72. Heise, N., A. L. S. Gutierrez, K. A. Mattos, C. Jones, R. Wait, J. O. Previato, and L. Mendonca-Previato. 2002. Molecular analysis of a novel family of complex glycoinositolphosphoryl ceramides from *Cryptococcus neoformans*: structural differences between encapsulated and acapsular yeast forms. *Glycobiology.* **12:** 409–420.
73. Adams, J., and Q. Ann. 1993. Structure determination of sphingolipids by mass spectrometry. *Mass Spectrom. Rev.* **12:** 51–85.
74. Singh, B. N., C. E. Costello, and D. H. Beach. 1991. Structures of glycophosphosphingolipids of *Tritrichomonas foetus*: a novel glycophosphosphingolipid. *Arch. Biochem. Biophys.* **286:** 409–418.
75. Costello, C. E., and J. E. Vath. 1990. Tandem mass spectrometry of glycolipids. *Methods Enzymol.* **193:** 738–768.